# Statistical mechanics of the quantum *K*-satisfiability problem

Sergey Knysh[1,*] and Vadim N. Smelyanskiy[2,†]
[1]*ELORET Corporation, NASA Ames Research Center, MS 229-1, Moffett Field, California 94035-1000, USA*
[2]*NASA Ames Research Center, MS 269-1, Moffett Field, California 94035-1000, USA*
(Received 31 March 2008; published 24 December 2008)

We study the quantum version of the random *K*-satisfiability problem in the presence of an external magnetic field $\Gamma$ applied in the transverse direction. We derive the replica-symmetric free-energy functional within the static approximation and the saddle-point equation for the order parameter: the distribution $P[h(m)]$ of functions of magnetizations. The order parameter is interpreted as the histogram of probability distributions of individual magnetizations. In the limit of zero temperature and small transverse fields, to leading order in $\Gamma$ magnetizations $m \approx 0$ become relevant in addition to purely classical values of $m \approx \pm 1$. Self-consistency equations for the order parameter are solved numerically using a quasi–Monte Carlo method for $K=3$. It is shown that for an arbitrarily small $\Gamma$ quantum fluctuations destroy the phase transition present in the classical limit $\Gamma=0$, replacing it with a smooth crossover transition. The implications of this result with respect to the expected performance of quantum optimization algorithms via adiabatic evolution are discussed. The replica-symmetric solution of the classical random *K*-satisfiability problem is briefly reexamined. It is shown that the phase transition at $T=0$ predicted by the replica-symmetric theory is of continuous type with atypical critical exponents.

DOI: 10.1103/PhysRevE.78.061128 PACS number(s): 02.50.−r, 75.10.Nr, 75.10.Jm, 03.67.Ac

## I. INTRODUCTION

The quantum phase transition (QPT) is a transition between different ground states driven by quantum fluctuations and controlled by certain parameters—for example, an external magnetic field. Study of QPTs in systems with strongly interacting spins attracted attention in the field of quantum computing due to the possibility of creating massively entangled states at the quantum critical point [1] and the relevance of QPTs to the analysis of the performance of quantum algorithms for solving classical combinatorial optimization problems (COPs) [2–6]. Quantum mechanics offers an alternative to the mechanism of thermal fluctuations for the transitions between states, which can be exploited in optimization procedures [2,7]. The QPT in this paper will be studied in the context of a general-purpose quantum adiabatic algorithm (QAA) proposed by Farhi and co-workers [8]. In its simplest form the algorithm is defined via a quantum *N*-spin Hamiltonian that is a sum of two terms:

$$\hat{H} = \mathcal{H}_{\mathrm{cl}}(\hat{\sigma}_i^z, \ldots, \hat{\sigma}_N^z) - \Gamma \sum_{i=1}^{N} \hat{\sigma}_i^x. \tag{1}$$

The first operator term is derived from a cost (energy) function of classical spins $\mathcal{H}_{\mathrm{cl}}(s_1, \ldots, s_N)$ by replacing each classical spin $s_i = \pm 1$ with a Pauli matrix, $\hat{\sigma}_i^z$. The ground state of this operator encodes the solution of a classical COP described by $\mathcal{H}_{\mathrm{cl}}$. The second term describes spin coupling to the external magnetic field $\propto \Gamma$ applied in the transverse direction (e.g., along the positive *x*-axis). At the start of the algorithm, $\Gamma$ is made very large and the ground state of $\hat{H}(0)$ is prepared with all spins pointing in the $\hat{x}$ direction. Then $\Gamma = \Gamma(t)$ is slowly reduced to zero, while the state of the quantum system remains close to the instantaneous adiabatic ground state of $\hat{H}(t)$—provided that the condition $\langle \Psi_0 | \frac{\partial}{\partial t} \hat{H} | \Psi_0 \rangle \ll (E_1 - E_0)^2$ is satisfied. Here $\hat{H}(t)|\Psi_n(t)\rangle = E_n(t)|\Psi_n(t)\rangle$. At the end of the algorithm at $\Gamma=0$, the system is found in a state which is a superposition of spin configurations corresponding to all degenerate global minima of $\mathcal{H}_{\mathrm{cl}}$. The run time of the algorithm is proportional to $1/g_{\min}^2$, where $g_{\min} = \min_{\Gamma}[E_1 - E_0]$ is a minimum of the energy gap [9] taken over the range of $\Gamma$.

It was noticed several decades ago that the properties of the solution space of complex COPs are closely related to those of spin-glass systems [10,11] It was also recognized [12] that many of the spin-glass models are in almost one-to-one correspondence with computationally hard COPs encountered in practice and forming a class of NP-hard [13] problems.

Whereas theoretical computer science is mostly concerned with the worst-case complexity, from the statistical physics perspective the main interest lies in the typical running time of algorithms over the random ensemble of problem instances (or samples of spin-glass systems) [11,14]. When this expected run time scales exponentially with the number of spins, the COP is considered intractable. This intractability was linked to so-called threshold phenomena [15–18] in NP-complete problems. In the physics community, these threshold phenomena were recognized as phase transitions in models of classical spin glasses [19]. Many NP-complete problems, including the most basic of them—random *K*-satisfiability (or *K*-SAT)—correspond to infinite-range *dilute* spin-glass models with *K*-local interactions [i.e., $\mathcal{H}(s_1, \ldots, s_N)$ is given by a sum of interaction terms, each involving a set of *K* spins chosen at random from a set of size *N*]. In this paper we study the quantum version of *K*-SAT. Quantum effects enter via the transverse field $\Gamma$ (for a different model of *K*-SAT with "quantum clauses" see Ref. [20]).

*Sergey.I.Knysh@nasa.gov
†Vadim.N.Smelyanskiy@nasa.gov

 

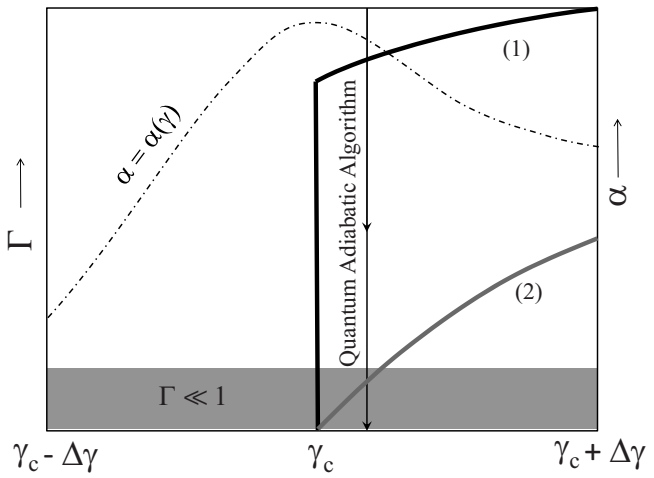


FIG. 1. Thick black (1) and gray (2) lines show two possible forms of quantum phase diagrams on the transverse field $\Gamma$ vs connectivity $\gamma$ plane for the random $K$-SAT problem. Black line (1) corresponds to the quantum dilute ferromagnet. The gray solid rectangle shows the region of interest in this paper with small transverse fields, $\Gamma \ll 1$. The dot-dashed line depicts the scaled exponent $\alpha=\alpha(\gamma)$ of the median run time $\mathcal{T}$ of a classical algorithm, $\mathcal{T}\sim\exp(\alpha N)$, over an ensemble of problem instances with the same $\gamma$.

In contrast to finite-dimensional models, the topology of links corresponding to spin couplings in $K$-SAT is completely random, with no nontrivial correlations. The random ensembles of instances are described by a single parameter, the connectivity $\gamma$, which is the number of interaction terms per spin, $\gamma=M/N$. The probability for a given spin to be involved in $d$ interactions is Poissonian with the finite mean value of $d$ equal to $K\gamma$. This is different from infinite-range fully connected spin models such as the Sherrington-Kirkpatrick model [21], where the value of $d=N-1$ scales with the number of spins.

Classical infinite-range spin-glass models in the dilute limit have been studied, though recent results concentrate on the zero-temperature limit [22–28]. However, very little is known about their respective quantum versions [described by the Hamiltonian (1) with $\mathcal{H}_{\rm cl}$ corresponding to an infinite-range dilute spin glass] despite a lot of interest in these models from the perspective of quantum computing. Recently, quantum versions of random exact cover and other related optimization problems have been studied [29] using a generalized annealing approximation [30]. At the same time, fully connected infinite-range quantum spin models have been analyzed in the literature using various approximations. This includes quantum versions of the Sherrington-Kirkpatrick (SK) [31–35], random Heisenberg [36], $p$-spin and random energy models [37]. Exact solutions in quantum spin glasses are mainly limited to one-dimensional models [38,39].

Numerical studies [16] have demonstrated that the typical run time of known classical algorithms applied to ensembles of randomly generated instances of $K$-SAT and similar models, as a function of $\gamma$, peaks at the point of static transition, which is a major bottleneck of classical optimization algorithms (see Fig. 1). This can be understood by analogy with the critical slowing down of the dynamics in the vicinity of phase transitions in problems without disorder. Similarly, we expect that the dynamics of the QAA for random $K$-SAT could be governed by the corresponding QPT. If the system underwent a QPT as the value of $\Gamma$ is lowered from a large value to 0, the gap would attain its minimum value at the point of the transition. The critical exponent associated with the singularity of the free energy would determine the scaling of the minimum gap (which would have the form of an exponential or stretched exponential [39]).

In this paper we concentrate on the static transition that corresponds to the satisfiability transition at zero temperature. We concentrate on $K=3$ as the most interesting case. It is the smallest value of $K$ for which $K$-SAT is NP-complete. Moreover, random $K$-SAT undergoes a random first-order phase transition for $K\geqslant 3$. As is the case with all random first-order transitions, the static transition is preceded by the dynamic transition. Results for similar model—$K$-XOR-SAT or dilute $p$-spin glass—at finite temperature indicate [40] that the free energy remains analytic across the dynamic transition, which would imply that the static transition is the real bottleneck of the simulated annealing algorithm. While giving credence to the idea of the analysis of the static transition, this picture may not necessarily apply to $K$-SAT for $K=3$, where the dynamic transition is accompanied by another, condensation, transition [27,28]. Due to difficulties of replica-symmetry-breaking analysis in the quantum case, we have only performed a replica-symmetric analysis. Although the replica-symmetric approximation is capable of correctly capturing the existence and qualitative properties of the static transition, it fails to describe the dynamic transition and overestimates the critical threshold $\gamma_c$.

In Fig. 1 we sketch two conjectured forms of the QPT line $\Gamma=\Gamma_c(\gamma)$. One possiblity is that $\Gamma_c(\gamma)$ changes continuously from the value of 0 at $\gamma=\gamma_c$. Alternatively, it may exhibit a finite jump [i.e., $\Gamma_c(\gamma_c)=\Gamma_{c0}>0$] as in dilute transverse Ising models without frustration [41,42]. Another (third) possibility is that the phase transition at $\Gamma=0$ disappears for any finite $\Gamma>0$. One may distinguish between these cases by setting $\Gamma\ll 1$ and studying the free energy for a range of values of $\gamma$ containing $\gamma_c$, as shown in Fig. 1. In the QAA the parameter $\Gamma(t)$ decreases with time, corresponding to a vertical line in the $(\gamma,\Gamma)$ plane as shown in Fig. 1. The central result of this paper is that it is the third possibility that takes place: quantum effects (the transverse field $\Gamma$) in the QAA Hamiltonian (1) make the static phase transition disappear; the free energy becomes analytical in the vicinity of $\gamma_c$ for small but finite $\Gamma$.

It should be mentioned in passing that certain highly symmetric examples of COPs have been constructed [43,44], where the total spin is an exact quantum number of the Hamiltonian $\hat{H}$ of Eq. (1) and the QAA fails due to the onset of a large spin tunneling through a broad, order $N$, semiclassical barrier with amplitude that scales down exponentially with $N$ [44,45]. However, in spin glasses, quantum evolution does not correspond to large spin dynamics. Instead, an exponentially large (in $N$) number of deep local minima of the classical energy are connected by an extremely large number of tunneling paths with amplitudes proportional to high powers of $\Gamma$. This picture as well as the analysis of QPTs is more relevant for understanding the typical complexity of the QAA for NP-hard problems such as $K$-SAT.

This paper is organized as follows. Section II presents a brief overview of important results for the classical version of random *K*-SAT and discusses the relationship between the present work's replica-symmetric analysis of quantum *K*-SAT and that of the classical *K*-SAT corresponding to the limit of $\Gamma=0$. We formulate the quantum version of *K*-SAT and analyze it using replica-symmetric theory in Sec. III. This is followed by an analysis of small magnetic fields $\Gamma$ in Sec. IV. In Sec. V we reexamine the classical $T=0$ random *K*-SAT to demonstrate that the replica-symmetric analysis predicts a continuous phase transition; it was previously thought to be of random first-order type. In Sec. VI we present the numerical results for both finite-temperature classical *K*-SAT and zero-temperature quantum *K*-SAT. We concentrate on $K=3$, which is the most interesting case. Since we utilize the replica-symmetric approximation in the analysis of quantum *K*-SAT, we compare these results with those predicted by the replica-symmetric theory for finite-temperature classical *K*-SAT (despite the fact that the tools to study replica symmetry breaking in classical *K*-SAT have appeared recently). In the Conclusion we discuss our results, especially in relation to the QAA and describe possible extensions of the present work. A novel quasi–Monte Carlo algorithm used in numerical calculations is described in the Appendix.

## II. CLASSICAL STATISTICAL MECHANICS OF RANDOM *K*-SAT: MONASSON-ZECCHINA REPLICA-SYMMETRIC SOLUTION AND ITS CONNECTION TO THE PRESENT WORK

An instance of random *K*-SAT is a system of *N* classical spins with the energy function that is written as a sum of *M* terms:

$$\mathcal{H}_{\mathrm{cl}}(s_1,\ldots,s_N)=\sum_{\boldsymbol{e}=(i_1,\ldots,i_K)<\mathcal{E}} E(s_{i_1},\ldots,s_{i_K};\boldsymbol{J}_{\boldsymbol{e}}). \tag{2}$$

Each term is associated with a *K*-tuple $\boldsymbol{e}=(i_1,\ldots,i_K)$. If spins labeled by $i=1,\ldots,N$ are viewed as vertices of some graph, *K*-tuples $\boldsymbol{e}$ correspond to its hyperedges. The set of all hyperedges for a given instance is denoted $\mathcal{E}$. Hyperedges corresponding to each term are chosen independently and uniformly at random; hence, with each instance of random *K*-SAT we may associate the realization of a random hypergraph. This represent the geometric part of disorder.

Each term defines a constraint involving spin variables $s_{i_1},\ldots,s_{i_K}$. The cost function $E(s_1,\ldots,s_K)$ can be either zero or some positive value representing the energy penalty for those combinations $(s_1,\ldots,s_K)$ that violate the constraint.

For *K*-SAT the constraints penalize exactly one out $2^K$ assignments. The cost function is chosen in the following form:

$$E_{\boldsymbol{J}}(s_1,\ldots,s_K)=2\prod_{\ell=1}^{K}\frac{1+J_\ell s_\ell}{2}. \tag{3}$$

Here $\boldsymbol{J}=(J_1,\ldots,J_K)$, where $J_\ell=\pm 1$, denotes the combination of *K* spin values that is assigned an energy penalty of 2.[1] The argument $\boldsymbol{J}$ of the cost function will be written as a subscript unless it refers to a specific hyperedge as in Eq. (2). The values of the *disorder variables* $\boldsymbol{J}_{\boldsymbol{e}}$ are chosen independently and uniformly at random for each constraint. The corresponding probability distribution assigns the probability of $1/2^K$ to each realization of $\boldsymbol{J}$:

$$p(\boldsymbol{J})=\prod_{\ell=1}^{K}\frac{\delta(J_\ell-1)+\delta(J_\ell+1)}{2}. \tag{4}$$

The energy (2) equals twice the number of violated constraints. When the number of constraints, *M*, is sufficiently small, all of them may be satisfied at the same time and the energy is zero. The properties of random *K*-SAT are studied in the limit when the number of variables, *N*, and constraints, *M*, goes to infinity, while the constraint-to-variable ratio $\gamma=M/N$ is kept constant. In this limit the fraction of variables involved in *d* constraints is Poissonian with mean $K\gamma$,

$$f_d(K\gamma)=\frac{1}{d!}(K\gamma)^d e^{-K\gamma}, \tag{5}$$

so that each variable appears in $K\gamma$ constraints on average.

It has been shown by computer studies that there exists a threshold $\gamma_c$ such that with overwhelming probability, there exists a configuration of *N* spins with zero energy if and only if $\gamma<\gamma_c$ (in the limit of large *N*). In the language of statistical mechanics, the random *K*-SAT undergoes a phase transition between the satisfiable (SAT) and unsatisfiable (UNSAT) phases at $\gamma=\gamma_c$. The interaction term (3) imposes a "weak" constraint on the spins involved in it. For this reason, unlike the Viana-Bray model with Ising interactions, the phase transition for random *K*-SAT does not coincide with the percolation transition for the corresponding hypergraph. For 3-SAT, the percolation transition takes place at $\gamma_{\mathrm{perc}}=1/6$, while the "experimental" value of the satisfiability threshold is $\gamma_c\approx 4.2$ [16]. The exact value of $\gamma_c$ for random *K*-SAT for $K\geqslant 3$ is not known.

Random *K*-SAT can be formulated as a statistical mechanics problem by introducing the artificial temperature $T=1/\beta$ and writing the Gibbs free energy

$$F=-\frac{1}{N\beta}\ln\sum_{\{s_i\}\in\{\pm 1\}^N} e^{-\beta\mathcal{H}_{\mathrm{cl}}(\{s_i\})}. \tag{6}$$

The extra factor of $1/N$ ensures that this is the free energy *per spin* so that *F* does not scale with *N*. It is related to the total internal energy E and the total entropy $\Sigma$ via the standard identity:

[1]This value of the energy of a violated constraint is an arbitrary quantity; it is often chosen to be equal to 2 only to simplify calculations [24,25].

$$F = \frac{1}{N}(\mathrm{E} - T\Sigma). \tag{7}$$

In the limit $T=0$ thermal fluctuations disappear and the second term in Eq. (7) vanishes. In this limit E converges to the minimum value of energy $\mathcal{H}_{\mathrm{cl}}$. Therefore, $F=0$ for $\gamma < \gamma_c$. Note that in random $K$-SAT there is no region where the minimum number of violated constraints is $o(N)$ except in the immediate vicinity of $\gamma_c$. For $\gamma > \gamma_c$ this number is $O(N)$ and $F>0$.

Instance-to-instance fluctuations of $F$ are small: $o(1)$. Therefore, with overwhelming probability a randomly chosen instance has free energy within $o(1)$ from $\langle F \rangle$, which is the disorder-averaged value. This is the central quantity which is computed using the replica method. We briefly discuss the main results obtained in [22,23]. The authors demonstrated that the disorder-averaged free energy of random $K$-SAT corresponds to the extremal value of the free-energy functional

$$\mathcal{F}[P(h)] = \gamma \int_{-\infty}^{\infty} dh_1 \cdots \int_{-\infty}^{\infty} dh_K P(h_1) \cdots P(h_K) \times \langle \mathcal{U}_{\boldsymbol{J}}(h_1, \ldots, h_K) \rangle_{\boldsymbol{J}} - \int_{-\infty}^{\infty} dh |h| \int_{-\infty}^{\infty} \frac{d\omega}{2\pi} e^{i\omega h} \tilde{P}(\omega)[1 - \tilde{P}(\omega)]. \tag{8}$$

Here $\langle \cdots \rangle_J$ denotes averaging over the parameters $J_\ell = \pm 1$ $(\ell = 1, \ldots, K)$ with equal weights assigned to all $2^K$ possibilities. The function $\mathcal{U}_{\boldsymbol{J}}(\{h_\ell\})$ is defined as

$$\mathcal{U}_{\boldsymbol{J}}(h_1, \ldots, h_K) = 2 \min(1, (J_1 h_1)_+, \ldots, (J_K h_K)_+). \tag{9}$$

Here and throughout the paper we use a shorthand $(\cdots)_+$, which we define as follows:

$$(x)_+ = \begin{cases} x & \text{for } x > 0, \\ 0 & \text{for } x \leqslant 0. \end{cases} \tag{10}$$

The function $\tilde{P}(\omega)$ in (8) is the Fourier transform of the distribution $P(h)$:

$$\tilde{P}(\omega) = \int_{-\infty}^{\infty} dh e^{-i\omega h} P(h). \tag{11}$$

The function $P^*(h)$ is found by extremizing $\delta\mathcal{F}[P(h)]$ subject to the constraint $\int_{-\infty}^{+\infty} dh\, P^*(h) = 1$. Distribution $P^*(h)$ has the meaning of the histogram of effective fields $h_i$ associated with each spin. Whenever $h_i \neq 0$ spin $s_i$ takes the same value $s_i = \operatorname{sgn} h_i$ in all spin configurations with the lowest energy. The absolute value $|h_i|$ is one-half of the energy cost needed to flip it.

The fraction of frozen (such that $h_i \neq 0$) spins $q = \int_{-\infty}^{-0} dh\, P^*(h) + \int_{+0}^{+\infty} dh\, P^*(h)$ is the order parameter associated with the satisfiability transition. In the satisfiable phase $q=0$, corresponding to $P^*(h) = \delta(h)$, whereas the unsatisfiable phase is described by finite $q>0$.

The simplest solution $P^*(h)$ of the extremality condition for the functional (8) is [22]

$$P(h) = \sum_{k=-\infty}^{+\infty} e^{-K\gamma(q/2)^{K-1}} I_{|k|}(K\gamma(q/2)^{K-1}) \delta(h-k), \tag{12}$$

where $I_k(x)$ is the modified Bessel function of first kind. The value of $q$ may be determined self-consistently from

$$1 - q = e^{-K\gamma(q/2)^{K-1}} I_0(K\gamma(q/2)^{K-1}). \tag{12a}$$

For $K=3$ and $\gamma > \gamma_d \approx 4.667$, Eq. (12a) has two stable solutions: the trivial $q=0$ and the nontrivial $q>0$. The nontrivial solution does not becomes stable until $\gamma > \gamma_c \approx 5.181$. The corresponding bound is very close to the annealed bound of $\gamma_{\mathrm{ann}} = \ln 2 / \ln(7/8) \approx 5.191$ and greatly overestimates the "experimental" value of the satisfiability threshold, $\gamma_{\mathrm{expt}} \approx 4.2$, from computer simulations [16].

A similar integer-$\delta$-peak solution [46] for the order parameter in the Viana-Bray model [47] was shown to be unstable in the longitudinal sector (i.e., within the replica-symmetric ansatz) [48]. The longitudinally stable solution exhibited a continuous part in addition to $\delta$ peaks. Though the appearance of the continuous component is believed to signal the breakdown of replica symmetry, the replica-symmetric result may still be useful if regarded as a type of variational approximation.

The incorporation of the continuous component led to an improved upper bound of the satisfiability transition $\gamma_c \approx 4.60$ obtained numerically [23]. This problem will be reexamined in Sec. V, and we will show that although the value of $\gamma_c$ had been determined correctly, the phase transition predicted by the replica-symmetric theory is actually continuous rather than first order as was claimed in Ref. [23].

Subsequent analysis by Mézard and Zecchina of one-step replica symmetry breaking (RSB) in random $K$-SAT improved the bound for the satisfiability threshold to $\gamma_c \approx 4.267$ [24,25]. It is believed that this one-step RSB solution is stable. What made the $T=0$ RSB analysis tractable (and yet required a lot of numerical effort) was the integer-$\delta$-peak ansatz for the distribution of effective fields *within each pure state*. It is a daunting task to extend one-step RSB analysis to finite temperatures (where noninteger effective fields are certain to exist), let alone including quantum effects. This paper only considers the replica-symmetric solution.

Using replica-symmetric analysis to study the quantum problem may have some merit. It has been argued in the literature [49], based in part on results on the quantum SK model [32,50], that effects of quantum tunneling may stabilize the replica-symmetric solution. Even if true, such symmetry must break down for extremely small transverse fields $\Gamma = o(N)/N$ or in the limit $\Gamma/T \ll 1$. Indeed, the purely classical limit $\Gamma = 0$ should be described by the one-step RSB solution obtained in Ref. [25].

## III. REPLICA SOLUTION OF QUANTUM $K$-SAT

### A. Replica-symmetric free-energy functional

The quantum Hamiltonian given by Eq. (1) is a sum of two terms: the purely classical term describing the interaction of Ising spins and the quantum term describing the cou-

pling to the external magnetic field applied in the transverse direction. By employing a Suzuki-Trotter transformation, the problem of finding the partition function $Z=\mathrm{Tr}\, e^{-\beta\hat{H}}$ can be reformulated as that of computing the partition function of the purely classical model. The corresponding classical partition function is written as a sum over all possible paths $s_i(t)$:

$$Z(\{\boldsymbol{J}\}) = \sum_{[\{s_i(t)\}]} \exp\left( - \int_0^\beta dt \mathcal{H}_{\mathrm{cl}}(\{s_i(t)\}) + \sum_i \mathcal{K}[s_i(t)] \right), \tag{13}$$

where the functional $\mathcal{K}[s(t)]$ is given by

$$\mathcal{K}[s(t)] = -\frac{1}{2} \ln(\tanh \Gamma \Delta t) \sum_{t=0,\Delta t,\ldots,\beta-\Delta t} s(t)s(t+\Delta t) + \frac{1}{2} \ln\left( \frac{1}{2} \sinh 2\Gamma \Delta t \right). \tag{13a}$$

The time variable $t$ takes $L$ discrete values $t=k\Delta t$ ($\Delta t = \beta/L$). Periodic boundary conditions $s_i(\beta)=s_i(0)$ are assumed.

The sum (13) is over $N\times L$ spin variables labeled by $i=1,\ldots,N$ and $t\equiv k\Delta t$. In anticipation of the limit $L\to\infty$ that will be taken eventually, we treat time as a continuous variable. In particular, we write $\int_0^\beta dt \cdots$ to mean $\Sigma_{k=0}^{L-1}\Delta t \cdots$. We use square brackets for writing functionals and for indicating sets labeled by continuous variables. Sets indexed by a discrete variable will be designated using curly braces. To avoid ambiguities we may adorn brackets or braces with subscripts and superscripts to indicate index variables and ranges ( e.g., $[\{s_i(t)\}_i]_{t=0}^{\beta}$).

A constant in expression (13a) ensures proper normalization of the statistical sum (13). It can be verified that (13) reduces to $Z^{(0)}=(2\cosh\beta\Gamma)^N$ for the noninteracting problem ($\mathcal{H}_{\mathrm{cl}}\equiv 0$).

We choose to write the classical Hamiltonian (2) in the following form:

$$\mathcal{H}_{\mathrm{cl}} = \sum_{i_1<i_2<\ldots<i_K} c_{i_1,\ldots,i_K} E(s_{i_1},\ldots,s_{i_K};\boldsymbol{J}_{i_1,\ldots,i_K}), \tag{14}$$

where the cost function $E_{\boldsymbol{J}}(s_1,\ldots,s_K)$ for $K$-SAT is given by Eq. (3). Disorder variables $\boldsymbol{J}_{i_1,\ldots,i_K}$ are assumed to be uniformly distributed according to Eq. (4).

The value of $c_{i_1,\ldots,i_K}$ is chosen to be 1 if the instance contains a constraint involving a set of variables $i_1,\ldots,i_K$ and zero otherwise. Random variables $c_{i_1,\ldots,i_K}$ are statistically independent and distributed according to

$$p(c) = \left(1 - \frac{K!\gamma}{N^{K-1}}\right)\delta(c) + \frac{K!\gamma}{N^{K-1}}\delta(c-1). \tag{15}$$

In the asymptotic limit ($N\to\infty$) the number of constraints will be $M=\gamma N$. The form (14) is preferable to (2) because it emphasizes the mean-field character of random $K$-SAT.

In this paper we will keep the derivation as general as possible. Formulas written without expanding (3) will be—by substituting appropriate expressions for $E_{\boldsymbol{J}}(s_1,\ldots,s_K)$ and $p(\boldsymbol{J})$—directly generalizable to any random combinatorial optimization problem with binary variables and $K$-local interaction (e.g., $K$-XOR-SAT, $K$-NAE-SAT, 1-in-$K$ SAT).

The central physical quantity of interest is the disorder-averaged value of the free energy $\langle F\rangle = -\frac{1}{N\beta}\langle \ln Z\rangle$. This is the same as the value of the free energy for a typical realization of disorder, the free energy (in contrast to $Z$) being a self-averaging quantity. We use the replica method to perform the disorder averaging. The average of the logarithm is rewritten using the following identity:

$$\langle \ln Z\rangle = \lim_{n\to 0} \frac{\partial}{\partial n}\langle Z^n\rangle. \tag{16}$$

For integer $n$, $Z^n$ is the partition function of a system of $n$ noninteracting replicas of the original random instance. Computing $\langle F\rangle$ will require performing the analytical continuation in $n$. The gist of the method is that disorder averaging in the expression for $\langle Z^n\rangle$ is done prior to performing the sum over classical spin configurations.

$$\langle Z^n\rangle = \sum_{[\{s_i^a(t)\}]} \exp\left( \sum_{a,i} \mathcal{K}[s_i^a(t)] \right) \times \left\langle \exp\left( - \sum_a \int_0^\beta dt \mathcal{H}_{\mathrm{cl}}(\{s_i^a(t)\}) \right) \right\rangle, \tag{17}$$

where the replica index $a$ runs from 1 to $n$, effectively increasing the number of spin variables to $N\times L\times n$.

Disorder averaging couples together formerly noninteracting replicas. However, it also transforms the dilute model with strong $O(1)$ interactions into a completely connected model with weak $O(1/N^{K-1})$ interactions. This permits the exact evaluation of the sum over the spin variables using mean-field theory. We express the mean-field solution in terms of a set of order parameters: spin correlation functions

$$Q_{a_1,\ldots,a_p}(t_1,\ldots,t_p) = \frac{1}{N}\sum_i s_i^{a_1}(t_1)s_i^{a_2}(t_2)\cdots s_i^{a_p}(t_p). \tag{18}$$

In the thermodynamic limit, the partition function (17) can be written in the form of a functional integral:

$$\langle Z^n\rangle = \int \mathcal{D}Q\, \mathcal{D}\lambda\, e^{-Nn\beta\mathcal{F}[\{Q\},\{\lambda\}]}. \tag{19}$$

The argument of the exponential is (up to a factor) the free-energy functional $\mathcal{F}$ that depends on correlation functions $\{Q_{a_1,\ldots,a_p}(t_1,\ldots,t_p)\}$ as well as Lagrange multipliers $\{\lambda_{a_1,\ldots,a_p}(t_1,\ldots,t_p)\}$ that enforce constraints (18). In Eq. (19) we have suppressed indices and time arguments for conciseness; similarly, $\mathcal{D}Q$ and $\mathcal{D}\lambda$ are a shorthand for multiple functional integrals.

In the limit $N\to\infty$ the integral (19) is dominated by the saddle-point value of $\mathcal{F}$:

$$F = -\frac{1}{Nn\beta}\ln\langle Z^n\rangle = \mathcal{F}[\{Q^*\},\{\lambda^*\}]. \tag{20}$$

The right-hand side is evaluated for $\{Q_{\boldsymbol{a}}^*(\mathbf{t})\}$ and $\{\lambda_{\boldsymbol{a}}^*(\mathbf{t})\}$, which make $\mathcal{F}$ stationary with respect to small variations. Note that in the following we will use a calligraphic $\mathcal{F}$ to

indicate a functional and an italic $F$ to denote its value at the saddle point.

In practice, working with an infinite set of time-dependent correlation functions is infeasible. Instead, as often done in the analysis of quantum spin glasses [32,36], we resort to the static approximation. We solve stationarity condition for the reduced set of functions—those that are independent of time arguments. Note that consistency requires that if $Q_{a_1,\ldots,a_p}(t_1,\ldots,t_p)$ are replaced by their static counterparts $Q_{a_1,\ldots,a_p}$, any time dependence be ignored for $\lambda_{a_1,\ldots,a_p}(t_1,\ldots,t_p)$ as well. Implemented in this form, the static approximation may be regarded as a type of variational approximation.

Integrating out $\{\lambda_{a_1,\ldots,a_p}\}$, we may write $\mathcal{F}(\{Q\})$ as a function of $\{Q_{a_1,\ldots,a_p}\}$ alone. It may be verified that static $Q_{a_1,\ldots,a_p}$ are the time-averaged dynamic correlation functions:

$$Q_{a_1,\ldots,a_p}=\frac{1}{\beta^p}\int dt_1\cdots dt_p Q_{a_1,\ldots,a_p}(t_1,\ldots,t_p). \quad (21)$$

We work within the replica-symmetric ansatz, which posits that $Q_{a_1,\ldots,a_p}$ at the saddle point of $\mathcal{F}$ are symmetric with respect to permutations of replicas. Due to this symmetry, not all $Q_{a_1,\ldots,a_p}$ are independent. The value of $Q_{a_1,\ldots,a_p}$ may only depend on the set of numbers $k_1,k_2,\ldots$, which, respectively, indicate the number of distinct replica indices that appear exactly once, twice, etc. We will write

$$Q_{a_1,a_2,\ldots,a_{k_1},b_1,b_1,b_2,b_2,\ldots,b_{k_2},b_{k_2},\ldots}=Q_{k_1,k_2,\ldots}, \quad (22)$$

where $\{a_i\},\{b_i\},\ldots$ are all distinct. Although for finite integer $n$ the inequality $\Sigma_r k_r\leq n$ must hold, performing the analytical continuation to $n\to 0$ requires knowledge of $\langle Z^n\rangle$ for all integer values of $n$. Thus, paradoxically, in the limit $n\to 0$, the values $k_r$ may run from 1 to $\infty$.

Note that in the classical limit $\Gamma=0$, only two paths $[s(t)\equiv+1$ and $s(t)\equiv-1]$ contribute to (17). Due to that, the static approximation becomes exact in this limit, and the order parameters $Q_{\{k_r\}}$ may depend only on $p=\Sigma_r k_{2r+1}$ as evidenced from Eq. (18). It has been recognized in the analysis of the classical Viana-Bray model by Kanter and Sompolinsky [46] that the order parameters $Q_p$ are the moments of the probability distribution $P(m)$ of average spin magnetizations. For a quantum model, $Q_{\{k_r\}}$ are related to the functional distribution $P[h(m)]$, where functions $h(m)$ are defined on the interval $[-1;1]$:

$$Q_{\{k_r\}}=\int [dh(m)]P[h(m)]\prod_{r=1}^{\infty}\left(\frac{\int dm\, e^{-\beta h(m)}m^r}{\int dm\, e^{-\beta h(m)}}\right)^{k_r}. \quad (23)$$

That the right-hand side of (23) is a functional integral is indicated by the use of square brackets ($\int[dh(m)]\cdots$). Such notation is customary in quantum field theory (see, e.g., [51]) and is consistent with our practice of using square brackets to indicate sets indexed by continuous variables. Regular multidimensional integrals will be written using curly braces (e.g., $\int\{dm_i\}_{i=1}^k\cdots$). Note that integrals over magnetizations run from $-1$ to $+1$.

We refer to the functions $h(m)$ as *effective fields*. It can be guessed from the form of (23) that these effective fields represent probability distributions of individual spin magnetizations via $p_i(m)\propto e^{-\beta h(m)}$. The distribution $P[h(m)]$ is the histogram of effective fields $h_i(m)$ associated with each spin. It may be interpreted as a probability distribution of probability distributions of magnetizations. Such constructs appear in replica analysis of classical problems in the description of RSB. As one can see, in the quantum case they are already present at the replica-symmetric level. Note that the effective fields $h(m)$ are defined only up to a shift by an arbitrary constant $h(m)\to h(m)+\text{const}$.

We express $\mathcal{F}(\{Q_{\{k_r\}}\})$ in terms of the distribution $P[h(m)]$ as a sum of two terms, which we will call a "quasipotential" $\mathcal{V}$ and a "quasientropy" $\mathcal{S}$, themselves dependent on $P[h(m)]$:

$$\mathcal{F}[\![P[h(m)]]\!]=\gamma\mathcal{V}[\![P[h(m)]]\!]-\mathcal{S}[\![P[h(m)]]\!]. \quad (24)$$

We have used double square brackets to indicate that arguments of $\mathcal{F}$, $\mathcal{V}$, and $\mathcal{S}$ are functionals. We refer the reader to supplementary materials [52] for mathematical details of replica calculations; here, we only provide the resulting expressions. For the quasipotential $\mathcal{V}[\![P[h(m)]]\!]$ we obtain

$$\mathcal{V}=\int[\{dh_\ell(m)\}_{\ell=1}^K]\prod_{\ell=1}^K P[h_\ell(m)]\langle\mathcal{U}_{\boldsymbol{J}}[\{h_\ell(m)\}]\rangle_{\boldsymbol{J}}, \quad (25)$$

where $\langle\cdots\rangle_{\boldsymbol{J}}$ indicates averaging over $2^K$ possible realizations of the vector $\boldsymbol{J}$. The functional integral over $h_1(m),\ldots,h_K(m)$ describes averaging over probability distributions $P[h_\ell(m)]$ of the *quasipotential density* $\mathcal{U}_{\boldsymbol{J}}[h_1(m),\ldots,h_K(m)]$ given by the following expression:

$$\mathcal{U}_{\boldsymbol{J}}[\{h_\ell(m)\}]=\frac{1}{\beta}\sum_{\ell=1}^K\ln\int dm\, e^{-\beta h_\ell(m)}-\frac{1}{\beta}\ln\int\{dm_\ell\}_{\ell=1}^K\times\exp\left(-\beta\hat{E}_{\boldsymbol{J}}(m_1,\ldots,m_K)-\beta\sum_{\ell=1}^K h_\ell(m_\ell)\right). \quad (26)$$

Integrals over magnetizations run from $-1$ to $+1$. We write $\int\{dm_\ell\}_{\ell=1}^K\cdots$ to indicate the $K$-dimensional integral over magnetizations $m_1,\ldots,m_K$.

The function $\hat{E}_{\boldsymbol{J}}(m_1,\ldots,m_K)$ that appears in Eq. (26) is multilinear in $m_1,\ldots,m_K$ and coincides with $E_{\boldsymbol{J}}(\cdots)$ when $\{m_\ell\}\in\{\pm1\}^K$. These two conditions determine it uniquely. For $K$-SAT the expression is obtained by formally replacing the discrete spin variables in Eq. (3) with continuous magnetizations $\{m_\ell\}$:

$$\hat{E}_{\boldsymbol{J}}(m_1,\ldots,m_K)=2\frac{1+J_1m_1}{2}\cdots\frac{1+J_Km_K}{2}. \quad (27)$$

It is easily seen that for any $\ell$ one may write $\hat{E}_{\boldsymbol{J}}(m_1,\ldots,m_K)=A_\ell+B_\ell m_\ell$, where $A_\ell$ and $B_\ell$ are independent of $m_\ell$, but depend on $\boldsymbol{J}$ and other magnetizations $\{m_{\ell'}\}_{\ell'\neq\ell}$.

For the quasientropy $\mathcal{S}[\![P[h(m)]]\!]$, we obtain the following expression:

$$\mathcal{S} = \int [dh(m)]\mathcal{L}[h(m)] \int [d\omega(m)] \times \exp\left( i \int dm\ \omega(m)h(m) \right) \tilde{\Sigma}[\omega(m)], \tag{28}$$

with $\tilde{\Sigma}[\omega(m)]$ given by

$$\tilde{\Sigma} = \tilde{P}[\omega(m)]\left( 1 - i \int dm\ \omega(m)u_0(m) - \ln \tilde{P}[\omega(m)] \right), \tag{28a}$$

which in turn is written in terms of the functional Fourier transform of $P[h(m)]$, which we denote $\tilde{P}[\omega(m)]$. It is implied that the normalization inside the functional integral over $\omega(m)$ is such that the inverse Fourier transform of $\tilde{P}[\omega(m)]$ reproduces $P[h(m)]$—i.e., $\int [d\omega(m)] \exp(i \int dm\ \omega(m)h(m)) \tilde{P}[\omega(m)] = P[h(m)]$.

The functional $\mathcal{L}[h(m)]$ is given by the following expression:

$$\mathcal{L}[h(m)] = -\frac{1}{\beta} \int dm\, e^{-\beta h(m)}. \tag{29}$$

The function $u_0(m)$ that appears in Eq. (28a) is entirely due to the kinetic term $\mathcal{K}[s(t)]$. In the limit of continuous magnetizations ($L \to \infty$) it can be evaluated in closed form:

$$e^{-\beta u_0(m)} = \frac{\beta\Gamma}{\sqrt{1-m^2}} I_1(\beta\Gamma\sqrt{1-m^2}) + \delta(m-1) + \delta(m+1). \tag{30}$$

Observe that in the limit $\Gamma = 0$ only contributions from $m = \pm 1$ are expected. It can be demonstrated that the free-energy functional (24) may be reexpressed, using the reduced order parameter $P(h)$, in the form given by Eq. (8).

It would seem from the form of Eq. (19) that the free energy should correspond to the minimum of the free-energy functional (24). Because of the peculiar nature of the limit $n \to 0$, this is not the case. It can be shown [52] that in the classical limit ($\Gamma = 0$) the free energy is a local *maximum* with respect to symmetric perturbations of $P(h)$ [i.e., such that $\delta P(-h) = \delta P(h)$] and a local *minimum* with respect to antisymmetric perturbations [such that $\delta P(-h) = -\delta P(h)$]. The quantum case is considerably more complex; fortunately, we only need to make sure that $P[h(m)]$ makes the free-energy functional $\mathcal{F}$ stationary and do not care whether it is a minimum or a maximum.

A few notes must be made about approximations made in this section. The assumption of replica symmetry is justified for sufficiently small connectivities $\gamma$; above the replica-symmetry-breaking transition ($\gamma > \gamma_{\mathrm{RSB}}$), it becomes an approximation. In contrast, the static approximation is not guaranteed to be exact anywhere except $\Gamma = 0$. It is a type of mean-field approximation, whereby fluctuating spins are replaced by average magnetizations.

The physical interpretation of the static approximation is rather intuitive. One can define the effective classical model with discrete spins replaced by *continuous* magnetizations $m_i \in [-1;1]$. For a specific realization of disorder,

$$Z(\{\boldsymbol{J}\}) = \int \{dm_i\}_{i=1}^{N} e^{-\beta \mathcal{H}_{\mathrm{eff}}(\{m_i\};\{\boldsymbol{J}\})}, \tag{31}$$

where the effective Hamiltonian $\mathcal{H}_{\mathrm{eff}}(\{m_i\};\{\boldsymbol{J}\})$ is

$$\mathcal{H}_{\mathrm{eff}} = \sum_{(i_1,\ldots,i_K)} \hat{E}_{\boldsymbol{J}}(m_{i_1},\ldots,m_{i_K};\boldsymbol{J}_{i_1,\ldots,i_K}) + \sum_i u_0(m_i), \tag{31a}$$

where $\Sigma_{(i_1,\ldots,i_K)}$ denotes a sum over all hyperedges $c_{i_1,\ldots,i_K} = 1$. Magnetizations $m_i$ roughly correspond to expectation values $\langle \hat{\sigma}_i^z \rangle$. Equation (31) depends on $\Gamma$ indirectly through form of $u_0(m)$.

It is known that the replica-symmetric approximation on random hypergraphs [25] is exactly the Bethe-Peierls (BP) approximation [53]. It can be demonstrated that the BP approximation for the effective classical model of Eqs. (31) reproduces the replica-symmetric static free energy derived in this section. For an alternative derivation of the free energy of quantum $K$-SAT (via the BP approximation) and quantum belief propagation equations we refer the reader to the supplementary materials [52].

### B. Stationarity condition and the Monte Carlo method

To complete the derivation of the replica free energy we need to find $P[h(m)]$, which makes the free-energy functional $\mathcal{F}[\![P[h(m)]]\!]$ stationary with respect to small variations; its value will be the desired free energy $F$, formally a function of $\beta$, $\Gamma$, and $\gamma$. The stationarity condition may be written as follows:

$$\frac{\delta \mathcal{F}}{\delta P[h(m)]} \equiv \gamma \frac{\delta \mathcal{V}}{\delta P[h(m)]} - \frac{\delta \mathcal{S}}{\delta P[h(m)]} = \mathrm{const}. \tag{32}$$

The arbitrary constant appearing on the right-hand side of Eq. (32) is a Lagrange multiplier associated with the normalization condition $\int [dh(m)] P[h(m)] = 1$. Substituting expressions (25) and (28) we will formulate the equation that must be satisfied by the saddle-point value of $P[h(m)]$. Due to a remarkable cancellation, we will be able to write this self-consistency equation in a relatively simple form.

Due to the specific form of the functionals (25) and (26), we may express the variation of $\mathcal{V}$ in the following form:

$$\frac{\delta \mathcal{V}}{\delta P[h(m)]} = K\left( \int [du(m)] Q[u(m)] \mathcal{L}[h(m) + u(m)] - \mathcal{L}[h(m)] \right). \tag{33}$$

This identity can be used as a definition of a new functional $Q[u(m)]$. It is necessarily normalized to unity ($\int [du(m)] Q[u(m)] = 1$). We will see that its meaning is that of the probability distribution of $u(m) = u_{\boldsymbol{J}}(m;[\{h_\ell(m)\}_{\ell=2}^{K}])$, where

$$u_{\boldsymbol{J}}(m;[\{h_\ell(m)\}]) = \frac{1}{\beta}\left(\sum_{\ell=2}^{K} \ln \int dm\, e^{-\beta h_\ell(m)} - \ln \int \{dm_\ell\}_{\ell=2}^{K} \times \exp\left(-\beta \hat{E}_{\boldsymbol{J}}(m,m_2,\ldots,m_K) - \beta \sum_{\ell=2}^{K} h_\ell(m_\ell)\right)\right), \tag{34}$$

and under the assumption that $\boldsymbol{J}$ is uniformly distributed and $h_2(m),\ldots,h_K(m)$ are taken from $P[h(m)]$.

On the other hand, the variation of the quasientropy with respect to $P[h(m)]$ reads

$$\frac{\delta S}{\delta P[h(m)]} = -\frac{1}{\beta}\int [du(m)]\mathcal{L}[h(m)+u(m)] \times \int [d\omega(m)]\exp\left(i\int dm\, \omega(m)u(m)\right) \times \left(\ln \tilde{P}[\omega(m)] + i\int dm\, \omega(m)u_0(m)\right). \tag{35}$$

Combining Eqs. (33) and (35) uncovers the following system of self-consistency equations:

$$Q[u(m)] = \int [\{dh_\ell(m)\}_{\ell=2}^{K}] \prod_{\ell=2}^{K} P[h_\ell(m)] \times \langle \delta[u(m) - u_{\boldsymbol{J}}(m;[\{h_\ell(m)\}])]\rangle_{\boldsymbol{J}}, \tag{36a}$$

$$P[h(m)] = \int [d\omega(m)]\exp\left(i\int dm\, \omega(m)(h(m)-u_0(m))\right) \times \exp K\gamma\left(-1+\int [du(m)] \times \exp\left(i\int dm\, \omega(m)u(m)\right)Q[u(m)]\right). \tag{36b}$$

In (36a) we use a *functional* generalization of the $\delta$ function, defined so that $F[x(m)]=\int [dy(m)]F[y(m)]\delta[x(m)-y(m)]$. Note that Eq. (36b) may be written in an alternative form by expanding the exponential in the integrand ( the term corresponding to $d=0$ is $e^{-K\gamma}\delta[h(m)-u_0(m)]$):

$$P[h(m)] = \sum_{d=0}^{\infty} f_d(K\gamma) \int [\{du_k(m)\}_{k=1}^{d}] \prod_{k=1}^{d} Q[u_k(m)] \times \delta\left[h(m) - u_0(m) - \sum_{k=1}^{d} u_k(m)\right]. \tag{36b'}$$

The appearance of the Poisson distribution $f_d(\alpha)=\frac{\alpha^d}{d!}e^{-\alpha}$ is intimately related to the hypergraph model that we study, as it is the distribution of the degrees (number of incident hyperedges) of the vertices. From the form of Eqs. (36a) and (36b') it is apparent that $h(m)$ are properly associated with the vertices of the random hypergraph, whereas $u(m)$ correspond to its hyperedges.

The system of equations (36a) and (36b) can be solved iteratively. Starting from some initial distribution $P^{(0)}[h(m)]$, we may compute a sequence of $\{Q^{(r)}[u(m)]\}$ and $\{P^{(r)}[h(m)]\}$ by applying (36a) and (36b). The limiting distribution

$$P^*[h(m)] = \lim_{r\to\infty} P^{(r)}[h(m)] \tag{37}$$

must be a solution to the stationarity condition (32). The *value* of the free energy is obtained from $F=\gamma V-S$, where the quasipotential $V$ is found by substituting $P^*[h(m)]$ into (25), and the expression for the quasientropy $S$ is rewritten using self-consistency equations (36a) and (36b):

$$S = K\gamma \int [dh(m)du(m)]P^*[h(m)]Q^*[u(m)] \times (\mathcal{L}[h(m)] - \mathcal{L}[h(m)+u(m)]) + \int [dh(m)]P^*[h(m)]\mathcal{L}[h(m)]. \tag{38}$$

The iterative procedure described above lends itself to a straightforward implementation using a Monte Carlo method. Observe that both expressions (36a) and (36b') are written as averages over probability distributions $P[h(m)]$ and $Q[u(m)]$ and vectors $\boldsymbol{J}$. The Monte Carlo algorithm that we describe below represents the distributions $P[h(m)]$ and $Q[u(m)]$ as finite samples $\{h_i(m)\}_{i=1}^{N}$ and $\{u_i(m)\}_{i=1}^{N}$. [Implementation details of memory representation of *functions* $h(m)$ and $u(m)$ are not discussed here; we assume that it can be done without any loss in precision.] A single iteration step can be implemented as follows.

(i) Compute a sample $\{u_i(m)\}$. For each $i\in\{1,\ldots,N\}$, do the following.

(a) Choose $h_2(m),\ldots,h_K(m)$ from the set $\{h_i(m)\}$ uniformly at random.

(b) Choose a disorder vector $\boldsymbol{J}$ at random.

(c) Evaluate $u(m)=u_{\boldsymbol{J}}(m;[\{h_\ell(m)\}_{\ell=2}^{K}])$ using Eq. (34).

(ii) Compute an updated sample $\{h_i'(m)\}$. For each $i\in\{1,\ldots,N\}$, do the following.

(a) Choose a random integer $d$ from the Poisson distribution with parameter $K\gamma$.

(b) If $k=0$, let $h'(m)=u_0(m)$.

(c) Otherwise, choose $u_1(m),\ldots,u_d(m)$ from the set $\{u_i(m)\}$ uniformly at random.

(d) Evaluate $h'(m)$ using

$$h'(m) = u_0(m) + \sum_{k=1}^{d} u_k(m). \tag{39}$$

The convergence criterion for the algorithm is that step-to-step fluctuations be entirely due to the finiteness of $N$—i.e., that both the old $\{h_i(m)\}$ and the updated $\{h_i'(m)\}$ histograms sample the same probability distribution. This can be verified by the Kolmogorov-Smirnov test, for instance [54].

### C. Quantum limit ($T=0$, $\Gamma>0$)

A number of simplifications are possible in this limit. Since all integrals over magnetizations have the form $\int dm\, e^{-\beta f(m)}$, in the limit $\beta\to\infty$ they are dominated by the

minimum value of $f(m)$. The replica free-energy functional $\mathcal{F}[\![P[h(m)]]\!] \equiv \gamma \mathcal{V}[\![P[h(m)]]\!] - \mathcal{S}[\![P[h(m)]]\!]$ retains the form given by Eqs. (25) and (28), but expressions (26) and (29) for $\mathcal{U}_{\boldsymbol{J}}[\{h_\ell(m)\}]$ and $\mathcal{L}[h(m)]$ simplify to, respectively,

$$\mathcal{U}_{\boldsymbol{J}}[\{h_\ell(m)\}] = \min_{\{m_\ell\}} \left[ \hat{E}_{\boldsymbol{J}}(\{m_\ell\}) + \sum_{\ell=1}^{K} h_\ell(m_\ell) \right] - \sum_{\ell=1}^{K} \min_m [h_\ell(m)] \tag{40}$$

and

$$\mathcal{L}[h(m)] = \min_m [h(m)], \tag{41}$$

while Eq. (30) assumes the asymptotic form

$$u_0(m) = -\Gamma \sqrt{1-m^2}. \tag{42}$$

Self-consistency equations retain the form of Eqs. (36a) and (36b), but the expression for $u_{\boldsymbol{J}}(m;[\{h_\ell(m)\}])$ reduces to the following:

$$u(m) = \min_{m_2,\ldots,m_K} \left[ \hat{E}_{\boldsymbol{J}}(m,m_2,\ldots,m_K) + \sum_{\ell=2}^{K} h_\ell(m_\ell) \right] - \sum_{\ell=2}^{K} \min_m [h_\ell(m)]. \tag{43}$$

The physical meaning of the effective fields $h(m)$ is particularly evident in the limit $T=0$. The free energy corresponds to the minimum of the effective Hamiltonian of Eq. (31):

$$\mathcal{H}_{T=0}(\{m_i\};\{\boldsymbol{J}\}) = \sum_{(i_1,\ldots,i_K)} \hat{E}(m_{i_1},\ldots,m_{i_K};\boldsymbol{J}_{i_1,\ldots,i_K}) - \Gamma \sum_i \sqrt{1-m_i^2}. \tag{44}$$

In the limit $\Gamma \to \infty$ the free energy is dominated by the second term $F=-\Gamma$, which corresponds to a state with all spins completely polarized along the $\hat{x}$ direction. In the limit $\Gamma \to 0$ the free energy is expected to be $F \approx 0$ in the satisfiable phase and $F \gtrsim 0$ in the unsatisfiable phase.

For each spin, $h_i(m)$ is, up to a constant, the increase in energy if the magnetization of spin $i$ is set to $m$ (magnetizations of other spins are allowed to adjust).

It is possible to set up a deceptively simple system of equations for magnetizations $\{m_i^*\}$ corresponding to the minimum of (44). Solving $\partial \mathcal{H}_{T=0}/\partial m_i = 0$ we observe that $m_i^*$ may be represented in terms of scalar effective fields $h_i^*$ via

$$m_i^* = \frac{h_i^*}{\sqrt{\Gamma^2 + (h_i^*)^2}}, \tag{45}$$

while each $h_i^*$ is a sum of contributions $u_k$ from each hyperedge incident to vertex $i$. E.g., for $K$-SAT,

$$u_k^* = \prod_{\ell=1}^{K} \frac{1 + J_\ell m_{k\ell}^*}{2}. \tag{46}$$

The description of the problem in terms of the order parameter $P(h^*)$—the histogram of fields $h_i^*$—is effective for large values of $\Gamma$ where (44) has only one local minimum. However, in the limit of small $\Gamma$ the number of local minima becomes exponential in $N$, which is the essential reason for the introduction of the functional order parameter.

## IV. SMALL TRANSVERSE FIELD REGIME AT ZERO TEMPERATURE

For small values of the transverse field, the free-energy functional can be expanded in powers of $\Gamma$ around $\Gamma=0$ corresponding to the classical limit. When the limit $\Gamma=0$ is taken first followed by the limit $T=0$, the classical expression for the free energy (8) is obtained. We expect that the physically relevant value of the free energy (unlike that of the order parameter) cannot be affected by the order in which the limits are taken. It is instructive to verify that the same result is obtained when the limit $T=0$ is taken first, followed by $\Gamma=0$. Even though the effective field functions $h(m)$ will be finite everywhere in the interval $[-1;+1]$, the value of the free energy will be determined by the values $h_{\pm 1}$ attained on both ends of the interval.

As a first step, we demonstrate that the function $u_{\boldsymbol{J}}(m;[\{h_\ell(m)\}])$ is always convex. This convexity property is valid for arbitrary values of $\Gamma$. We evaluate $u(m)$ for some linear combination of magnetizations $m_0$ and $m_1$. Writing $m_2^*,\ldots,m_K^*$ to denote the values of magnetization that minimize the first term on right-hand side of Eq. (43) and using the property that $\hat{E}_{\boldsymbol{J}}(m_1,\ldots,m_K)$ is a multilinear function of magnetizations, we write the lengthy inequality proving the convexity of $u(m)$:

$$\begin{aligned} u(\alpha m_0 + (1-\alpha)m_1) &= \min_{m_2,\ldots,m_K} \left[ \hat{E}_{\boldsymbol{J}}(\alpha m_0 + (1-\alpha)m_1, m_2, \ldots, m_K) + \sum_{\ell=2}^{K} h_\ell(m_\ell) \right] - \sum_{\ell=2}^{K} \min_m [h_\ell(m)] \\ &= \alpha \left( \hat{E}_{\boldsymbol{J}}(m_0, m_2^*, \ldots, m_K^*) + \sum_{\ell=2}^{K} h_\ell(m_\ell^*) - \sum_{\ell=2}^{K} \min_m [h_\ell(m)] \right) \\ &\quad + (1-\alpha) \left( \hat{E}_{\boldsymbol{J}}(m_1, m_2^*, \ldots, m_K^*) + \sum_{\ell=2}^{K} h_\ell(m_\ell^*) - \sum_{\ell=2}^{K} \min_m [h_\ell(m)] \right) \\ &\geqslant \alpha u(m_0) + (1-\alpha) u(m_1). \end{aligned} \tag{47}$$

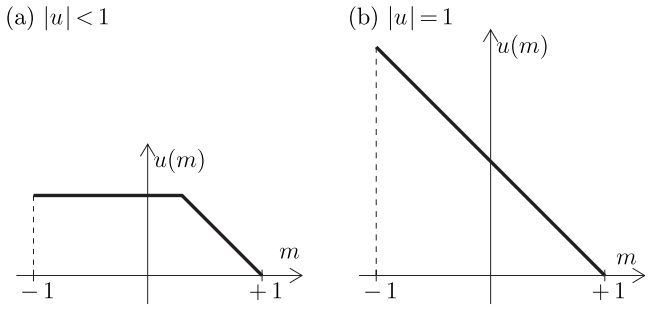


FIG. 2. Form of $u(m)$ in the classical limit ($\Gamma=0$). Two cases are depicted: (a) $|u|<1$, $u>0$ and (b) $|u|=1$, $u>0$. Analogous figures for $u<0$ may be obtained by mirror reflection $m\to -m$.

Using the convexity of $u(m)$, it can be established from Eq. (36b′) that in the limit $\Gamma=0$ the effective field functions $h(m)$ are also convex due to the vanishing of $u_0(m)$. The convexity of $h(m)$ and the multilinearity of $\hat{E}_{\boldsymbol{J}}(\{m_\ell\})$, together, ensure that expressions of the form $\hat{E}_{\boldsymbol{J}}(m_1,\ldots,m_K)+h_\ell(m_\ell)$ achieve their minimum values for $m_\ell=\pm 1$. Similarly, minima of effective fields $h(m)$ can be replaced by $\min(h_{-1},h_{+1})$ due to the convexity of $h(m)$. It follows that the value of the free energy will be unchanged if minima over the interval $m\in[-1;+1]$ are replaced with minima over the discrete set $m\in\{-1;+1\}$. Hence, the free energy of the quantum model in the limit $\Gamma=0$ must equal that of the classical model.

One corollary to this is that in the limit $\Gamma=0$ the functions $u(m)$ are piecewise linear. Indeed, $du/dm=(\partial/\partial m)\hat{E}_{\boldsymbol{J}}(m,m_2^*,\ldots,m_K^*)$ may depend on $m$ only indirectly via $\{m_\ell^*\}_{\ell=2}^K$. Since $m_\ell^*\in\{-1;+1\}$, the slope of $u(m)$ cannot change continuously; instead, it assumes one of finitely many values depending on the value of $m$.

So far, we have kept the derivation as general as possible. In the following we restrict our attention to random $K$-SAT proper described by the cost function (27). In the limit $\Gamma=0$ functions $u(m)$ (sketched in Fig. 2) may be parametrized by a single parameter $u$ as follows:

$$u(m)=\min(2,2|u|,1-(\operatorname{sgn} u)m). \tag{48}$$

Using the same letter for the function $u(m)$ and the parameter $u$ should not lead to confusion. We will always include the magnetization argument to refer to the function $u(m)$. The value of $u(m)$ for a particular magnetization (e.g., $m=0$ or $m=\pm 1$) will be indicated using subscripts: i.e., $u_0$, $u_{\pm 1}$.

It can be seen from Eq. (48) that $u=\frac{1}{2}(u_{-1}-u_{+1})$. Although $h(m)=u_0(m)+\Sigma_{k=1}^d u_k(m)$ does not admit a simple parametrization, we can still define the scalar $h=\frac{1}{2}(h_{-1}-h_{+1})$. This choice ensures that $h=\Sigma_{k=1}^d u_k$. As expected, $u(m)$ defined by Eq. (43) assumes the form of Eq. (48) and depends on $\{h_\ell(m)\}$ only via $\{h_\ell\}$:

$$u=\min(1,(J_2h_2)_+,\ldots,(J_Kh_K)_+), \tag{49}$$

with $(x)_+$ used to denote $\max(x,0)$.

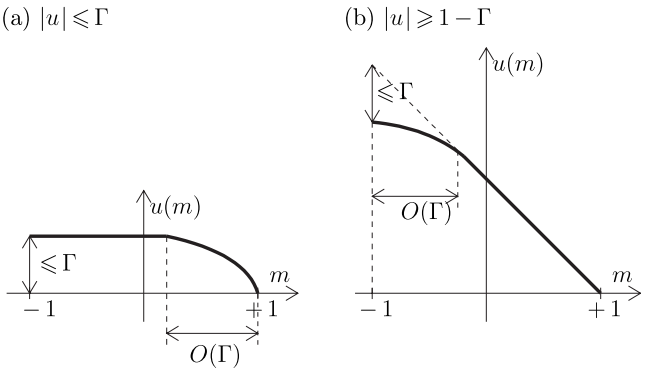


FIG. 3. Possible form of $u(m)$ for finite, but small $\Gamma$. The figures depict two possibilities corresponding to $u>0$ ($u<0$ corresponds to mirror images $m\to -m$): (a) $|u|\leqslant\Gamma/2$ and (b) $|u|\geqslant 1-\Gamma/2$. For $1\pm m=O(\Gamma)$, the functions $u(m)$ are not piecewise linear. Together with Fig. 2, this encompasses all possible forms of $u(m)$ in the limit of small $\Gamma$.

This describes two different regimes. The function $u(m)$ has the form depicted in Fig. 2 (left) whenever $\min_\ell\{(J_\ell h_\ell)_+\}<1$ and that shown on the right if $\min_\ell\{(J_\ell h_\ell)_+\}\geqslant 1$.

The order parameter $P[h(m)]$ may be obtained by iterating Eqs. (36a) and (36b) starting from, e.g., $P^{(0)}[h(m)]=\delta[h(m)-u_0(m)]$ corresponding to the noninteracting model.[2] The effects of small, but finite values of $\Gamma$ can be illustrated by performing a single iteration. Substituting $h_2(m)=\cdots=h_K(m)=u_0(m)$ into (43) gives

$$u_{\boldsymbol{J}}(m)=\min_{m_2,\ldots,m_K}\left[2\frac{1+J_1m}{2}\prod_{\ell=2}^K\frac{1+J_\ell m_\ell}{2}-(K-1)\Gamma\sqrt{1-m^2}\right]+(K-1)\Gamma. \tag{50}$$

This expression is neither zero (as in the classical case) nor even piecewise linear. It should be declared in advance that we do not need the precise analytical expression for $u_{\boldsymbol{J}}(m)$ as the free energy will not depend on such details. It is easily seen that $u_{\boldsymbol{J}}(m)$ is monotonic in $m$ and that it is zero at $m=-J_1$. In addition, one can demonstrate that

$$u_{\boldsymbol{J}}(m)=\Gamma-o(\Gamma)\quad\text{when } 1+J_1m\gg\Gamma. \tag{51}$$

When $K\geqslant 3$ this approximate identity is strengthened to $u_{\boldsymbol{J}}(m)=\Gamma$ for $1+J_1m\geqslant C\Gamma$ (for some constant $C$). This form of $u_{\boldsymbol{J}}(m)$ is sketched in Fig. 3 (left) for $J_1<0$ [in this particular case $u(0)=\Gamma$]. Since we are not concerned with the precise form of $u(m)$, it is still permissible to describe it using a single parameter $u=\frac{1}{2}(u_{-1}-u_{+1})$ (which would equal $-J_1\Gamma/2$ in the present case). Expression (48) would apply everywhere on $[-1;+1]$ except for the vicinity of $m=\operatorname{sgn} u$, where $1-(\operatorname{sgn} u)m=O(\Gamma)$. Note that if either $1-(\operatorname{sgn} u)m$

[2]When $\Gamma=0$, as $P^{(0)}[h(m)]=\delta[h(m)]$ could be a metastable solution. However, for finite $\Gamma$, successive iterations will always converge to the stable solution.

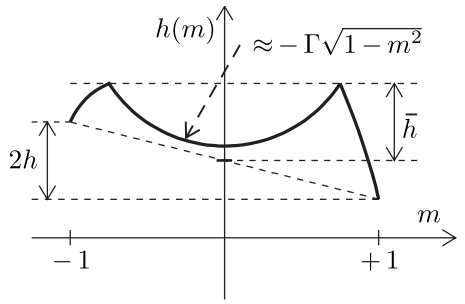


FIG. 4. Typical form of the function $h(m)$, parametrized by $h$ and $\bar{h}$. In general, $h=\frac{1}{2}(h_{-1}-h_{+1})$. The distance from the middle minimum at $m\approx 0$ to the center point of the line joining $h(-1)$ and $h(+1)$ is $\Gamma-\bar{h}$. All features $O(\Gamma^2)$ have been suppressed (see discussion in the text).

$\ll\Gamma$ or $1-(\mathrm{sgn}\,u)m\gg\Gamma$, expression (48) remains valid up to $o(\Gamma)$.

By considering additional iterations of Eqs. (36a) and (36b) it is possible to classify all possible forms of $u(m)$ that can be encountered. In addition to the piecewise linear forms of Fig. 2, it may have one of the forms depicted in Fig. 3. The latter form may occur only if $|u|\leqslant\Gamma/2$ (Fig. 2, left) or $1-\Gamma/2\leqslant|u|<1$ (Fig. 2, right).

Observe that Eq. (48) is approximately valid for all $m$, with the possible exception of $1-(\mathrm{sgn}\,u)m\gg\Gamma$. Recognizing that $u(m)$ is monotonic and that $|du/dm|\leqslant 1$, we can restate the condition in an equivalent form. We require that $du/dm$ approximately [up to $o(\Gamma)$] equal either 0 or $\pm 1$ for $1-|m|\gg\Gamma$. For values of $m$ such that $1-|m|=O(1)$ the derivative $du/dm$ equals either 0 or $\pm 1$ with a correction of at most $O(\Gamma^2)$.

To investigate the qualitative form of effective fields $h(m)$ write Eq. (39) substituting the value of $u_0(m)$:

$$h(m)=-\Gamma\sqrt{1-m^2}+\sum_{k=1}^{d}u_k(m). \tag{52}$$

The function $h(m)$ is a sum of one concave and $d$ convex functions. One of the possible forms of $h(m)$ is sketched in Fig. 4. All features that are $o(\Gamma)$ have been suppressed. In particular, Fig. 4 fails to reflect the fact that the locations of the local minima at $m=\pm 1$ are shifted by $O(\Gamma^2)$.

In general, local minima of $h(m)$ away from the end points of the interval $[-1;+1]$ must satisfy $dh/dm=0$. Since $du_k/dm$ are approximately integers for $1-(\mathrm{sgn}\,u)m\gg\Gamma$, such local minima can exist only if $\Sigma_k\,du_k/dm|_{m=0}\approx 0$ and can only be located at $m^*\approx 0$ [up to $O(\Gamma)$]. Neglecting contributions of $O(\Gamma^2)$ and higher, the free energy is determined by values of $u(m)$ and $h(m)$ at $m=0$ or $m=\pm 1$.

We will parametrize each of $u(m)$ and $h(m)$ by the scalars $u$, $\bar{u}$ and $h$, $\bar{h}$, respectively. We define

$$u=\frac{u_{-1}-u_{+1}}{2}, \tag{53a}$$

$$\bar{u}=\frac{u_{-1}-2u_0+u_{+1}}{2}. \tag{53b}$$

And $h$ and $\bar{h}$ parametrizing $h(m)$ of Eq. (52) are chosen as follows:

$$h=\sum_{k=1}^{d}u_k, \tag{54a}$$

$$\bar{h}=\sum_{k=1}^{d}\bar{u}_k. \tag{54b}$$

Note that $u$ and $\bar{u}$ are not independent variables, but are related by

$$\bar{u}=\min(|u|,1-|u|). \tag{55}$$

Combining Eqs. (48), (52), and (53), we obtain, for values of $h(m)$ at $m=\pm 1$ and $m=0$,

$$h_{\pm 1}=\sum_{k=1}^{d}|u_k|\pm h, \tag{56a}$$

$$h_0=\sum_{k=1}^{d}|u_k|+\bar{h}-\Gamma. \tag{56b}$$

The expression $\Sigma_{k=1}^{d}|u_k|$ represents a constant shift which must cancel out in the expression for the free energy. This cancellation allows one to parametrize $h(m)$ by $h$ and $\bar{h}$ alone.

It is straightforward to rewrite the self-consistency equations (36) in terms of the reduced distributions $P(h,\bar{h})$ and $Q(u,\bar{u})$. However, it is more instructive to derive self-consistency equations from the stationarity condition for the free-energy functional $\mathcal{F}[P(h,\bar{h})]$, which is obtained by using our ansatz for $h(m)$.

As before, we separate the free-energy functional into two parts corresponding to the quasipotential and quasientropy: $\mathcal{F}[P(h,\bar{h})]=\gamma\mathcal{V}[P(h,\bar{h})]-\mathcal{S}[P(h,\bar{h})]$. We write down without proof the expression for the quasientropy $\mathcal{S}[P(h,\bar{h})]$:

$$\mathcal{S}=\int dh\,d\bar{h}\mathcal{L}(h,\bar{h})\int\frac{d\omega\,d\bar{\omega}}{(2\pi)^2}e^{i\omega h+i\bar{\omega}\bar{h}}\tilde{\Sigma}(\omega,\bar{\omega}), \tag{57}$$

where $\mathcal{L}(h,\bar{h})$ and $\tilde{\Sigma}(\omega,\bar{\omega})$ are given by, respectively,

$$\mathcal{L}(h,\bar{h})=\max(|h|,\Gamma-\bar{h}), \tag{57a}$$

$$\tilde{\Sigma}(\omega,\bar{\omega})=\tilde{P}(\omega,\bar{\omega})[1-\ln\tilde{P}(\omega,\bar{\omega})], \tag{57b}$$

with $\tilde{P}(\omega,\bar{\omega})=\int dh\,d\bar{h}e^{-i\omega h-i\bar{\omega}\bar{h}}P(h,\bar{h})$ used to denote the Fourier transform of $P(h,\bar{h})$. The derivation of this expression is straightforward and relies on the ability to replace all minima over magnetizations in the interval $[-1;+1]$ by those over the discrete set $m\in\{0,\pm 1\}$.

The derivation of the quasipotential is slightly more intricate. The minimum of

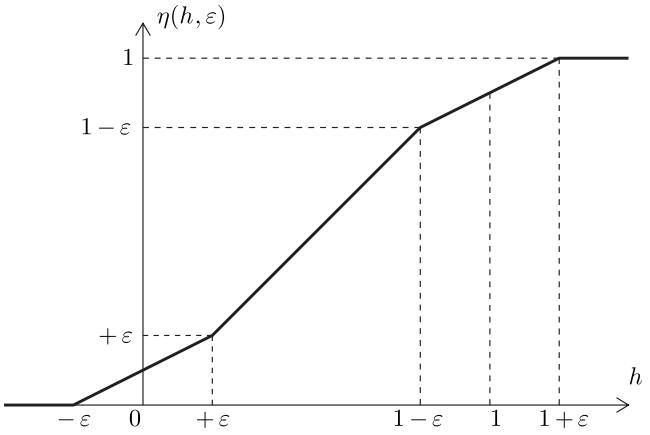


FIG. 5. The form of the function $\eta=\eta(h,\varepsilon)$ defined in Eq. (59b).

$$\hat{E}'_{\boldsymbol{J}}(m_1,\ldots,m_K)=2\prod_{\ell=1}^{K}\frac{1+J_\ell m_\ell}{2}+\sum_{\ell=1}^{K}h_\ell(m_\ell) \tag{58}$$

may occur only for $m_1,\ldots,m_K=0,\pm 1$. It is unnecessary to consider all $3^K$ possibilities, however. Let $m_\ell^*$ denote the location of a global minimum of $h_\ell(m)$. The location of the global minimum of (58) is such that $m_\ell=0$ or $m_\ell=-J_\ell$ for some $\ell$, while all other magnetizations are $m_{\ell'}=m_{\ell'}^*$. It is never advantageous to have more than one magnetization different from $m_\ell^*$ as long as $\Gamma<1$.

Therefore, $\hat{E}'_{\boldsymbol{J}}(m_1,\ldots,m_K)$ may be written as a minimum over just $K$ distinct possibilities. After some algebra we obtain the following expression for the quasipotential $\mathcal{V}[P(h,\bar{h})]$:

$$\mathcal{V}=\int\{dh_\ell d\bar{h}_\ell\}\prod_{\ell=1}^{K}P(h_\ell,\bar{h}_\ell)\langle\mathcal{U}_{\boldsymbol{J}}(\{h_\ell,\bar{h}_\ell\})\rangle_{\boldsymbol{J}}, \tag{59}$$

with $\mathcal{U}_{\boldsymbol{J}}(\{h_\ell,\bar{h}_\ell\})$ given by

$$\mathcal{U}_{\boldsymbol{J}}(\{h_\ell,\bar{h}_\ell\})=2\min_{\ell=1,\ldots,K}\{\eta(J_\ell h_\ell,\Gamma-\bar{h}_\ell)\}, \tag{59a}$$

and the definition of $\eta(h,\varepsilon)$ is

$$\eta(h,\varepsilon)=\min(1,(h)_+)+\frac{1}{2}(\varepsilon-|h|)_+-\frac{1}{2}(\varepsilon-|h-1|)_+ \tag{59b}$$

[the auxiliary function $\eta(h,\varepsilon)$ is sketched in Fig. 5 for illustrative purposes]. Note that for $\varepsilon\leqslant 0$, Eq. (59b) reduces to $\eta(h,\varepsilon)=\min(1,(h)_+)$.

It is immediately seen that in the limit $\Gamma=0$, Eqs. (57) and (59), rewritten in terms of $P(h)=\int d\bar{h}\,P(h,\bar{h})$, coincide with classical $T=0$ expressions for the quasientropy and quasipotential, respectively.

The stationarity condition is $\delta(\gamma\mathcal{V}-\mathcal{S})/\delta P(h,\bar{h})=\text{const}$. It should come as no surprise that the following identity holds:

$$\frac{\delta\mathcal{V}}{\delta P(h,\bar{h})}=K\left(\int du\,d\bar{u}Q(u,\bar{u})\mathcal{L}(h+u,\bar{h}+\bar{u})-\mathcal{L}(h,\bar{h})\right)+\text{const}, \tag{60}$$

where $Q(u,\bar{u})$ is effectively a distribution of just one parameter $u$:

$$Q(u,\bar{u})=Q(u)\delta(\bar{u}-\min(|u|,1-|u|)), \tag{61a}$$

$$Q(u)=\int\{dh_\ell d\bar{h}_\ell\}\prod_{\ell=2}^{K}P(h_\ell,\bar{h}_\ell)u_{\Gamma;\boldsymbol{J}}(\{h_\ell,\bar{h}_\ell\}_{\ell=2}^{K}), \tag{61b}$$

with $u_{\Gamma;\boldsymbol{J}}(h_2,\bar{h}_2;\ldots;h_K,\bar{h}_K)$ given by

$$u_{\Gamma;\boldsymbol{J}}(\{h_\ell,\bar{h}_\ell\})=\min_{\ell=2,\ldots,K}\{\eta(J_\ell h_\ell,\Gamma-\bar{h}_\ell)\}. \tag{61c}$$

Solving the stationarity condition reveals the following relationship between $P(h,\bar{h})$ and $Q(u,\bar{u})$:

$$P(h,\bar{h})=\int dh\,d\bar{h}\,e^{i\omega h+i\bar{\omega}\bar{h}}\exp K\gamma\tilde{Q}(\omega,\bar{\omega}), \tag{62}$$

where $\tilde{Q}(\omega,\bar{\omega})$ is the Fourier transform of $Q(u,\bar{u})$. An alternative form of (62) is

$$P(h,\bar{h})=\sum_d f_d(K\gamma)\int\{du_k d\bar{u}_k\}\prod_{k=1}^{d}Q(u_k,\bar{u}_k)\times\delta\left(h-\sum_{k=1}^{d}u_k\right)\delta\left(\bar{h}-\sum_{k=1}^{d}\bar{u}_k\right). \tag{62'}$$

The order parameter can be found by solving Eqs. (61a)–(61c) and (62) self-consistently. It is straightforward to write down belief propagation equations in the limit $\Gamma\ll 1$ for a particular disorder realization by "reverse-engineering" these relations, interpreting $P(h,\bar{h})$ and $Q(u,\bar{u})$ as the histograms of effective fields associated with vertices and hyperedges of the random hypergraph.

## V. CLASSICAL ZERO-TEMPERATURE SOLUTION REEXAMINED

The main goal of the present work is the study of the phase transition in quantum $K$-SAT at the replica-symmetric level. It is fair to compare those results with the results on finite-temperature $K$-SAT using same replica-symmetric approximation. The limiting cases $\Gamma=0$ or $T=0$ in both models correspond to zero-temperature $K$-SAT. It has been solved at the replica-symmetric level in Ref. [23]. (Moreover, a one-step RSB solution is also available [25,28].) However, we are forced to briefly reexame this problem. We will demonstrate that the longitudinally stable replica-symmetric order paramater changes continuously from zero across the phase transition in connectivity $\gamma$. This result contradicts the prediction of [23], that the order parameter jumps discontinuously. We believe that this apparent discontinuity of the order paramater is merely an artifact of discretization used in the numerical procedure.

In this section we consider the model described by the free-energy functional (8), but with the expression (9) modified to

$$\mathcal{U}_J^{(O)}(h_1,\ldots,h_K) = 2 \min_{\ell=1,\ldots,K} \{(J_\ell h_\ell)_+\}. \tag{63}$$

We will refer to this modified version as Model O. The original version will be called Model A.

The distinguishing feature of Model O is the absence of any explicit scale. The free-energy functional becomes covariant with respect to scaling transformation (rescaling of effective fields by a factor of $\lambda$):

$$\mathcal{F}^{(O)}[\lambda P(h/\lambda)] = \lambda \mathcal{F}^{(O)}[P(h)]. \tag{64}$$

The immediate consequence is that the maximum value of $\mathcal{F}^{(O)}[P(h)]$ can be either 0 or $+\infty$, depending on the value of $\gamma$.

Under successive iterations of self-consistency equations for $P(h)$ and $Q(u)$, the distribution quickly converges to a universal form, with any subsequent iterations merely rescaling effective fields by a factor of $\lambda$ that depends on the value of $\gamma$:

$$P^{(r+1)}(h) = \lambda P^{(r)}(h/\lambda). \tag{65}$$

The width of the distribution $\Delta = \int dh\, P(h)|h|$ serves as a simplified order parameter: it flows toward fixed points $\Delta^* = 0$ or $\Delta^* = +\infty$ for $\gamma < \gamma_c$ or $\gamma > \gamma_c$, respectively. The threshold $\gamma_c$ is determined from

$$\lambda(\gamma_c) = 1. \tag{66}$$

Note that this condition is equivalent to $\mathcal{F}[P^*(h)] = 0$, where the limiting distribution $P^*(h)$ has been rescaled so that it has finite nonzero weight. Both $P(h)$ and $Q(u)$ contain a $\delta$-function peak at zero as well as a continuous part:

$$P(h) = (1-q)\delta(h) + q\rho(h), \tag{67a}$$

$$Q(u) = \left[1 - \left(\frac{q}{2}\right)^{K-1}\right]\delta(u) + \left(\frac{q}{2}\right)^{K-1}\chi(u). \tag{67b}$$

The self-consistency condition for singular components of $P(h)$ and $Q(u)$ may be written as follows:

$$q = 1 - \exp\left(-\frac{K\gamma}{2^{K-1}} q^{K-1}\right). \tag{68}$$

A similar equation appears in the analysis of the leaf-removal algorithm for random $K$-XOR-SAT [55]. The correspondence becomes exact with the replacement $\gamma/2^{K-1} \to \gamma$. A nontrivial solution to Eq. (68) appears discontinuously above some threshold $\gamma_q$ ($\gamma_q \approx 3.276$ for $K=3$). However, this threshold is irrelevant for our problem, because the corresponding $\lambda(\gamma_q) < 1$. The value of $\gamma_c$ is determined from self-consistency equations for continuous parts:

$$\chi(u) = (K-1)\rho(u)\left(\int_{|u|}^{+\infty} dh\, \rho(h)\right)^{K-2}, \tag{69a}$$

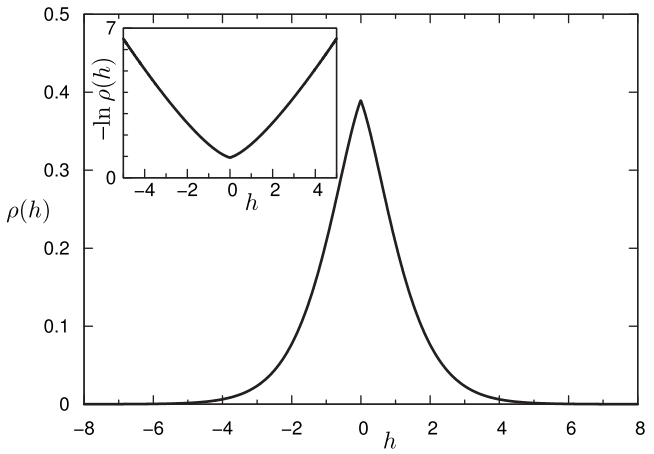


FIG. 6. Scale-free solution $\rho^*(h)$ of Eqs. (69) for $\tilde{\gamma} = \tilde{\gamma}_c$. The inset shows $\ln \rho(h)$ to illustrate the approximately exponential decrease of $\rho(h)$ as $h \to \infty$.

$$\rho(h) = \sum_{d=1}^{\infty} \frac{\tilde{\gamma}_c^d}{e^{\tilde{\gamma}_c} - 1} \int \{du_k\} \prod_{k=1}^{d} \chi(u_k)\, \delta\left(h - \sum_k u_k\right), \tag{69b}$$

where we have substituted $\lambda = 1$ (the "renormalized" connectivity is $\tilde{\gamma}_c = K\gamma_c q^{K-1}$). Solving these equations iteratively we obtain $\tilde{\gamma}_c \approx 3.1650$, which translates into $\gamma_c \approx 4.6002$, in agreement with [23]. In Fig. 6 we plot $\rho^*(h)$ at the critical value of $\gamma$.

It is not coincidental that the critical threshold in this simplified model is the same as in real $T=0$ classical $K$-SAT (Model A). The only difference between the two models is the interaction term

$$U_J^{(A)}(h_1,\ldots,h_K) = \min(2, U_J^{(O)}(h_2,\ldots,h_K)). \tag{70}$$

When the width of the distribution $\Delta \ll 1$, Models O and A are roughly equivalent. The only effect of this modification is to prevent the divergence of $\Delta^*$ for $\gamma > \gamma_c$.

The solution of Model O may serve as a variational ansatz for the solution of Model A, which will be increasingly precise as the transition is approached. We take $P_\Delta^*(h)$—the scale-invariant solution of Model O, appropriately rescaled to have width $\Delta$. The variational free energy may be written as follows:

$$F_{\text{var}}^{(A)}(\Delta) = (\gamma - \gamma_c)\mathcal{V}^{(O)}[P_\Delta^*(h)] - \gamma \int_1^\infty dh \left(\int_h^\infty dh'\, P_\Delta^*(h')\right)^K. \tag{71}$$

The asymptotic form of $P_\Delta^*(h)$ is related to that of $\rho^*(h)$ (see Fig. 6, inset):

$$\rho^*(h) \propto e^{-\mu(h)|h|}, \tag{72}$$

where $\mu(h)$ is a function of very slow growth. In particular, it grows slower than the iterated logarithm of $|h|$. Therefore, in the limit $\Delta \ll 1$, the correction term in (71) scales as $e^{-\mu(1/\Delta)/\Delta}$. Hence, the free energy may be written as follows:

$$F_{\text{var}}(\Delta) \approx \alpha(\gamma - \gamma_c)\Delta - e^{-\mu(1/\Delta)/\Delta}. \tag{73}$$

Solving $dF_{\text{var}}/d\Delta=0$ with respect to $\Delta$ yields

$$\gamma - \gamma_c \propto \frac{1}{\Delta^2} e^{-\mu(1/\Delta)/\Delta}. \tag{74}$$

With some abuse of notation (we write $x \sim y$ to mean that $x$ is asymptotically proportional to $y$ with the coefficient of proportionality being an extremely slow-varying function of $y$), the dependence of the order parameter $\Delta$ on connectivity $\gamma > \gamma_c$ may be written as follows:

$$\Delta \sim \frac{1}{|\ln(\gamma - \gamma_c)|}. \tag{75}$$

Given the extremely singular character of this function, it is not surprising that the transition looks like a first-order transition in numerical simulations. The critical exponents $\alpha=1$ and $\beta=0$ are precisely those expected for the first-order transition (the scaling exponent associated with the logarithm is zero). In the vicinity of the phase transition, just above it, the behavior of the free energy is

$$F \sim \frac{\gamma - \gamma_c}{|\ln(\gamma - \gamma_c)|}. \tag{76}$$

We corroborate this prediction by a numerical study. We are primarily interested in $\Delta(\gamma)$: the dependence of the order parameter on connectivity. However, the convergence of the Monte Carlo algorithm is too slow for $\gamma \approx \gamma_c$. The number of iterations of self-consistency equations for $P(h)$ and $Q(u)$ necessary to ensure convergence diverges near the phase transition. To avoid this problem, we compute the inverse $\gamma(\Delta)$. Instead of iterating self-consistency equations for fixed connectivity $\gamma$ until convergence of $\Delta$, we fix the width of the distribution $\Delta$ and tune the value of $\gamma$ at each step so that the width of $P(h)$ remains the same. With this approach, convergence of $\gamma$ is always complete (to within machine precision) in under 20 iterations.

In addition, the Monte Carlo procedure is replaced with a quasi–Monte Carlo procedure, which we have formulated specifically for problems involving probability distributions. The detailed description of the method is in the Appendix. The advantage of using the quasi–Monte Carlo method is a dramatic reduction of numerical error. All numerical results presented in this paper are obtained using this method.

In Fig. 7, we plot the function $\gamma(\Delta)$ obtained numerically. To establish that the phase transition is continuous, we must convince ourselves that $\gamma(\Delta)$ is a strictly increasing function of $\Delta$—i.e., that $\gamma(\Delta) > \gamma(0)$ for arbitrarily small $\Delta$. The inset shows the roughly linear dependence of $f(\gamma,\Delta)=[C - \ln \Delta^2(\gamma-\gamma_c)]^{-1}$ on $\Delta$ [cf. Eq. (74)] that, when extrapolated, predicts the vanishing of $\Delta$ as $\gamma \to \gamma_c$.

In Fig. 8, we plot the dependence of the free energy $F$ on connectivity $\gamma$ in the vicinity of $\gamma_c$. Contrary to visual perception, the slope of $F(\gamma)$ at $\gamma=\gamma_c+0$ is zero from Eq. (76). The "apparent" slope $\Delta F/\Delta\gamma$ decreases as a function of $\Delta\gamma$, as can be seen by comparing the main figure with the inset in Fig. 8.

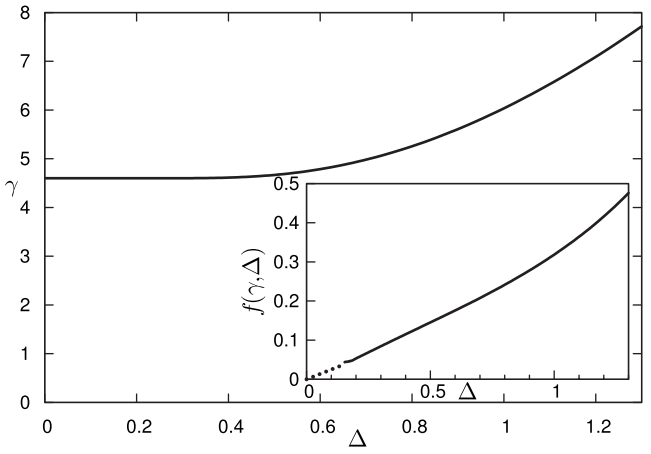


FIG. 7. Connectivity $\gamma$ vs width of the distribution of effective fields $\Delta$ in Model A. We predict that $\gamma > \gamma_c$ for any $\Delta > 0$, so $\Delta(\gamma)$ has no discontinuities. The inset replots the data to illustrate the asymptotic relation (74). The $y$-axis corresponds to $f(\gamma,\Delta)=[3.5 - \ln \Delta^2(\gamma-\gamma_c)]^{-1}$, which is asymptotically linear in $\Delta$ as $\Delta \to 0$. The dotted line is the result of extrapolation to small values of $(\gamma-\gamma_c)$ where the numerical error is too large.

## VI. NUMERICAL RESULTS

### A. A Classical regime ($\Gamma=0$, $T>0$)

In addition to Models O and A described in Sec. V, we introduce two new models: classical Models B and AB. Classical Model AB is precisely the finite-temperature classical random $K$-SAT. The distinguishing feature of Model B is the absence of explicit temperature. It is defined using Eqs. (25) and (28), but with the following choice for $\mathcal{U}_{\mathbf{J}}(\{h_\ell\})$ and $\mathcal{L}(h)$, respectively:

$$\mathcal{U}^{(B)} = -\ln\left(1 - \frac{1}{(1+e^{-2J_1 h_1})\cdots(1+e^{-2J_K h_K})}\right), \tag{77a}$$

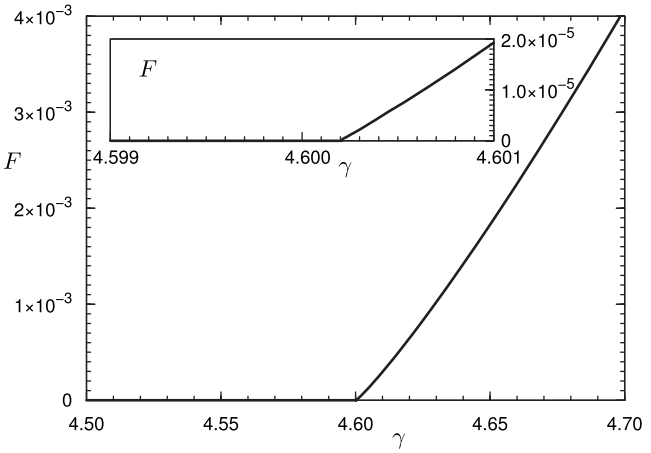


FIG. 8. Free energy $F$ vs connectivity $\gamma$. Contrary to visual perception, $F(\gamma)$ is *not* linear for $\gamma > \gamma_c$. The inset zooms in on the transition, keeping the aspect ratio the same. The apparent slope of $F(\gamma)$ in the inset is smaller. This apparent slope will tend to zero as progressively higher zoom ratios are used.

TABLE I. Four different models defined by the values taken by parameters $T$ and $\Lambda$. Statistical properties of Models O, A, and B should be similar, since $T/\Lambda=0$ in all three cases. Model AB is the classical finite-temperature random $K$-SAT.

| Type of model | Temperature | Scale $\Lambda$ |
|---|---|---|
| Model O | $T=0$ | $\Lambda=\infty$ |
| Model A | $T=0$ | $\Lambda=1$ |
| Model B (classical) | $T=1$ | $\Lambda=\infty$ |
| Model AB (classical) | $T>0$ | $\Lambda=1$ |

$$\mathcal{L}^{(B)} = \ln(2\cosh h). \tag{77b}$$

All four models (O, A, B, and AB) can be described by a single form of the free-energy functional that depends explicitly on two parameters: the temperature $T=1/\beta$ and the energy scale parameter $\Lambda$. This common model can be defined using the following expression for $\mathcal{U}_J(\{h_\ell\})$ and $\mathcal{L}(h)$:

$$\mathcal{U}_{T,\Lambda} = -T\ln\left(1-\frac{1-e^{-2\Lambda/T}}{\prod_{\ell=1}^{K}(1+e^{-2J_\ell h_{\ell'}/T})}\right), \tag{78a}$$

$$\mathcal{L}_{T,\Lambda} = T\ln\left(2\cosh\frac{h}{T}\right). \tag{78b}$$

We summarize the values of $T$ and $\Lambda$ for the four models we have introduced in Table I.

This common model with explicit dependence on $T,\Lambda$ satisfies the following scaling relations:

$$\mathcal{F}_{T,\Lambda}[P(h)] = T\mathcal{F}_{T=1,\Lambda}[TP(h/T)] \tag{79a}$$

$$= \Lambda\mathcal{F}_{T,\Lambda=1}[\Lambda P(h/\Lambda)]. \tag{79b}$$

The implication is that the statistical-mechanical properties of this model depend on the ratio of two scales $T/\Lambda$. In particular, we expect that Models O, A, and B undergo a phase transition at the same value of the critical connectivity, since $T/\Lambda=0$ in all three models. We have previously established that $\gamma_c^{(A)}=\gamma_c^{(O)}$.

The numerical results for the classical Model B are presented in Figs. 9 and 10. To obtain the numerical solution, we adopted the same strategy as for Model A. We computed $\gamma$ as well as a number of other quantities for each value of $\Delta$. An interesting feature of Model B is that the function $\gamma(\Delta)$ plotted in Fig. 9 is nonmonotonic and cannot be inverted unambiguously for $\gamma>\gamma^{(B)}(+\infty)$. Although not reflected in the figure, formally there exists another solution corresponding to $\Delta=+\infty$, with the free energy $F=+\infty(-\infty)$ for $\gamma>\gamma_c^{(O)}$ $(<\gamma_c^{(O)})$. Since a branch with the higher free energy must be chosen, the branch $\Delta^*<\Delta<+\infty$ is unstable and $F^{(B)}=+\infty$ for $\gamma>\gamma_c^{(O)}$.

Whereas the free energy $F^{(A)}$ of Model A (see Sec. II) corresponds to the internal energy E of Eq. (7) (or the number of violated constraints), the free energy of Model B is related to the entropy $\Sigma$:

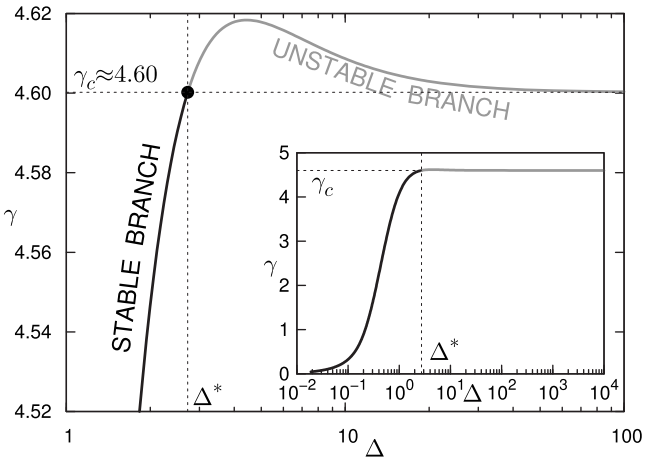


FIG. 9. Connectivity $\gamma$ vs width of distribution of effective fields $\Delta$ in classical Model B. The main figure shows $\gamma(\Delta)$ in the region close to critical. The inset shows $\gamma(\Delta)$ in a wider range. The branch $\Delta>\Delta^*$ is unstable; hence, $\Delta=+\infty$ as soon as $\gamma>\gamma_c$. The unstable branch is drawn with the gray solid line.

$$-NF^{(B)} = \langle\Sigma\rangle = \langle\ln\mathcal{N}_S\rangle, \tag{80}$$

where $\mathcal{N}_S$ represents the number of solutions that satisfy all constraints. The divergence of $F^{(B)}$ signals the transition to the unsatisfiable phase $(\mathcal{N}_S=0)$.

In Fig. 10 we plot the specific entropy (i.e., the negative of the free energy) as a function of $\Delta$. Note that since the entropy is finite at $\gamma=\gamma_c$, the number of solutions, just prior to the satisfiability transition, is exponentially large. It is the expected behavior: for the associated hypergraph, random graph theory [56] predicts that there are $O(N)$ vertices that are either isolated or belong to small isolated clusters. These

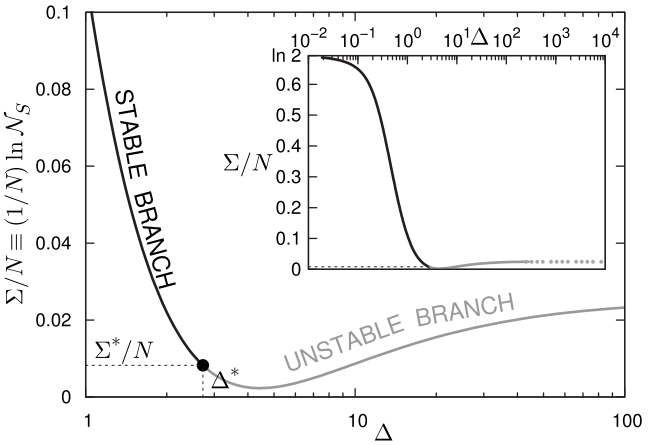


FIG. 10. Specific entropy $\Sigma/N$ (logarithm of the number of solutions) as a function of $\Delta$. The main figure shows the dependence in the critical region, while a wider range of $\Delta$ is used for the inset. The unstable branch $(\Delta>\Delta^*)$ is drawn in gray. The entropy decreases to $\Sigma^*$ as $\gamma$ approaches $\gamma_c$, but jumps to $-\infty$ (corresponding to zero solutions) for $\gamma>\gamma_c$. Entropy corresponding to very large values of $\Delta$ in the unstable branch could not be determined with good precision. Results of extrapolation are indicated using the dotted gray line.

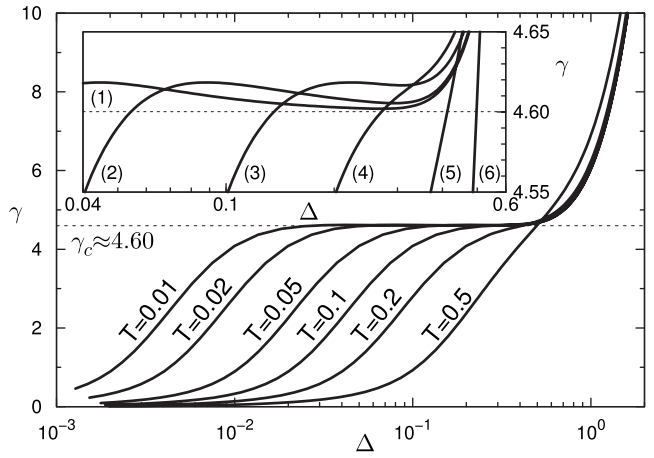


FIG. 11. The dependence $\gamma(\Delta)$ in classical Model AB for a range of temperatures. Curves labeled (1)–(6) in the inset correspond to temperatures $T=0.01$, 0.02, 0.05, 0.1, 0.2, and 0.5, respectively. The temperatures are labeled explicitly in the main figure. The curves smoothly interpolate between the regime of Model B $[\Delta=O(T)]$ and that of Model A $[\Delta=O(1)]$. The inset shows that $\gamma(\Delta)$ is not monotonic for sufficiently small temperatures.

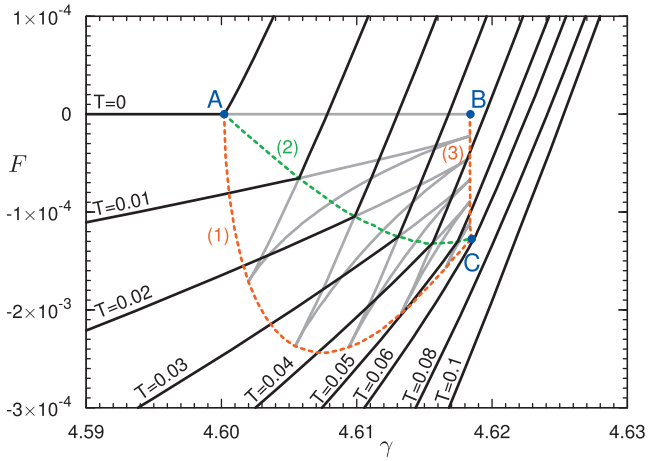


FIG. 12. (Color) Two-dimensional parametric plots $(\gamma(\Delta),F(\Delta))$ for classical Model AB (finite-temperature $K$-SAT). Different lines correspond to different temperatures. Black solid lines correspond to the stable branches of the free energy; gray lines correspond to unstable solutions. Switching between stable branches occurs along the green dashed line (2). Along this line, the first derivative $dF/d\gamma$ of the free energy has a discontinuity. Red dashed lines (1) and (3) are the spinodals $dV/dS=0$. Points $A$ and $B$ along $T=0$ line correspond, respectively, to the critical threshold in Model A and the metastable solution $\gamma\approx4.6184$ of Model B. Lines (1), (2), and (3) meet at a critical point $C$, corresponding to $T^*\approx0.05864$. Note that the line $BC$ is *nearly* vertical, with corrections that are $\sim\exp(-1/T)$.

make a finite contribution to the entropy, but do not affect the overall satisfiability of the random instance.

Based on results for Model B we expect that the nonmonotonic behavior of $\gamma(\Delta)$ persists for some sufficiently small but finite temperatures. In Fig. 11 we plot the functions $\gamma(\Delta)$ for the classical Model AB for a range of temperatures from $T=0.01$ to $T=0.5$. It is seen that far away from $\gamma=\gamma_c$ Model AB interpolates between the regimes of Model B with $\Delta=O(T)$ and Model A with $\Delta=O(1)$. For small temperatures $\gamma(\Delta)$ is nonmonotonic, which gives rise to the first-order phase transition.

We make two-dimensional parametric plots $(\gamma(\Delta),F(\Delta))$ for a range of temperatures $T$ (see Fig. 12). For $T<T^*$ these curves are self-intersecting. Stable branches (black solid lines) have a discontinuous slope at the point of self-intersection which leads to the discontinuity of the order parameter. The dashed green line [marked (2) in the figure] is the line of singularities between $(\gamma_c,0)$ and $(\gamma^*,F^*)$ terminating at the critical point. In the space of variables $(\gamma,T,F)$ stable and unstable branches of $F$ form a dovetail singularity. It should be recalled that for $T=0$ the derivative $dF/d\gamma$ has no discontinuity, although it is difficult to see from the figure.

Finally, in Fig. 13, we show the numerical phase diagram in the plane $(\gamma,T)$. The discontinuity of the order parameter becomes zero at both ends of the phase boundary between $(\gamma_c,0)$ and $(\gamma^*,T^*)$.

### B. Quantum regime ($\Gamma>0$, $T=0$)

We introduce quantum Model B and quantum Model AB as follows. We will keep the definition (57) for the quasientropy, but in the definition (59) for the quasipotential the function $\eta(h,\varepsilon)$ will be replaced with

$$\eta_\Lambda(h,\varepsilon)=\min(\Lambda,(h)_+)+\frac{1}{2}(\varepsilon-|h|)_+-\frac{1}{2}(\varepsilon-|h-\Lambda|)_+, \tag{81}$$

so that the free-energy functional will contain a characteristic scale of the effective fields $\Lambda$ explicitly. By choosing the values of $\Gamma$ and $\Lambda$ according to Table II we define the two quantum models: Models B and AB. The purely classical

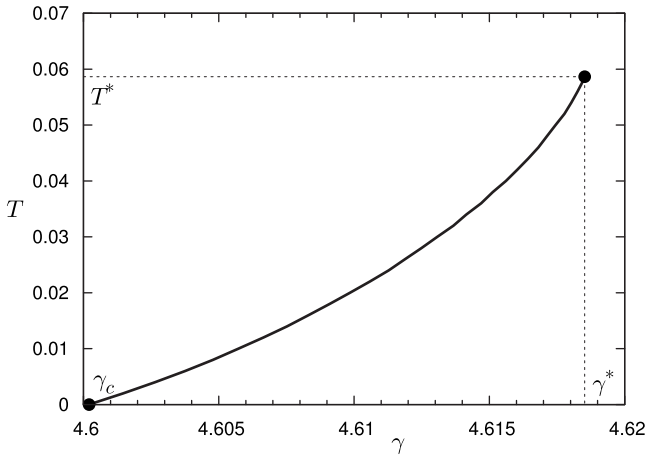


FIG. 13. Numerical phase digram of classical Model AB (finite-temperature $K$-SAT). The phase boundary (phase transition line) starts from $T=0$, critical connectivity $\gamma_c$, and terminates at the critical point with $\gamma^*\approx4.6185$ and $T^*\approx0.05864$.

TABLE II. Four different models defined by the values taken by parameters $\Gamma$ and $\Lambda$. Statistical properties of Models O, A, and B should be similar, since $\Gamma/\Lambda=0$ in all three cases. Model AB is quantum random *K*-SAT; we study the limit $\Gamma \ll 1$.

| Type of model | Transverse field | Scale $\Lambda$ |
|---|---|---|
| Model O | $\Gamma=0$ | $\Lambda=\infty$ |
| Model A | $\Gamma=0$ | $\Lambda=1$ |
| Model B (quantum) | $\Gamma=1$ | $\Lambda=\infty$ |
| Model AB (quantum) | $\Gamma>0$ | $\Lambda=1$ |

models–Models O and A–correspond to the limit $\Gamma=0$.

Ordinarily, the free energy of the quantum model corresponds to the smallest eigenvalue of the Hamiltonian. However, in the limit $\Lambda=+\infty$, where $\Lambda$ defines the energy scale of the classical Hamiltonian, the contribution from the states with energy $E>0$ vanishes. The value $F^{(B)}$ of the free energy for an instance of Model B may be evaluated using the degenerate perturbation theory. In the limit $\Lambda=+\infty$, this free energy is proportional to $\Gamma$, which can also be seen from scaling analysis. We choose $\Gamma=1$; the free energy $F^{(B)}$ is directly related to a property of the space of solutions $\boldsymbol{\sigma}$.

Consider a graph $\mathcal{G}$ having $\mathcal{N}_S$ vertices corresponding to spin configurations that satisfy all constraints. We draw edges between vertices of $\mathcal{G}$ corresponding to configurations $\boldsymbol{\sigma}$ and $\boldsymbol{\sigma}'$ that differ by a single spin flip. Let $\mathcal{A}$ denote the adjacency matrix for this graph—i.e.,

$$\mathcal{A}_{\boldsymbol{\sigma}\boldsymbol{\sigma}'} = \begin{cases} 1 & \text{if } d(\boldsymbol{\sigma},\boldsymbol{\sigma}')=1, \\ 0 & \text{if } d(\boldsymbol{\sigma},\boldsymbol{\sigma}')=0 \text{ or } d(\boldsymbol{\sigma},\boldsymbol{\sigma}')\geqslant 2, \end{cases} \tag{82}$$

where $d(\boldsymbol{\sigma},\boldsymbol{\sigma}')$ denotes the Hamming distance between spin configurations $\boldsymbol{\sigma}$ and $\boldsymbol{\sigma}'$. The free energy of Model B will be related to the norm of matrix $\mathcal{A}$:

$$-NF^{(B)} = \langle \|\mathcal{A}\| \rangle = \langle \lambda_{\max}(\mathcal{A}_{\boldsymbol{\sigma}\boldsymbol{\sigma}'}) \rangle \tag{83}$$

(the spectrum of $\mathcal{A}_{\boldsymbol{\sigma}\boldsymbol{\sigma}'}$ is symmetric).

The expression for the free energy may be simplified in the limit $\Lambda=+\infty$. Since in this limit $\bar{u}=|u|$ and $u$ is equally likely to be positive or negative, we may express the joint probability distribution $Q(u,\bar{u})$ in terms of the probability distribution of $\bar{u}$ denoted $Q_+(\bar{u})$:

$$Q(u,\bar{u}) = \frac{1}{2}[Q_+(\bar{u})\delta(u-\bar{u}) + Q_+(\bar{u})\delta(u+\bar{u})]. \tag{84}$$

Substituting this into Eq. (62), we obtain the following factorization of the joint distribution $P(h,\bar{h})$:

$$P(h,\bar{h}) = P_+\left(\frac{\bar{h}+h}{2}\right)P_+\left(\frac{\bar{h}-h}{2}\right), \tag{85a}$$

$$P_+(\bar{h}) = \int d\bar{h}\, e^{i\bar{\omega}\bar{h}} \exp\frac{K\gamma}{2}(\tilde{Q}_+(\bar{\omega})-1). \tag{85b}$$

We can use relations (84) and (85) to write the free energy as a functional of $P_+(\bar{h})$ alone. The resulting expression for $\mathcal{F}[P_+(h)]$ is

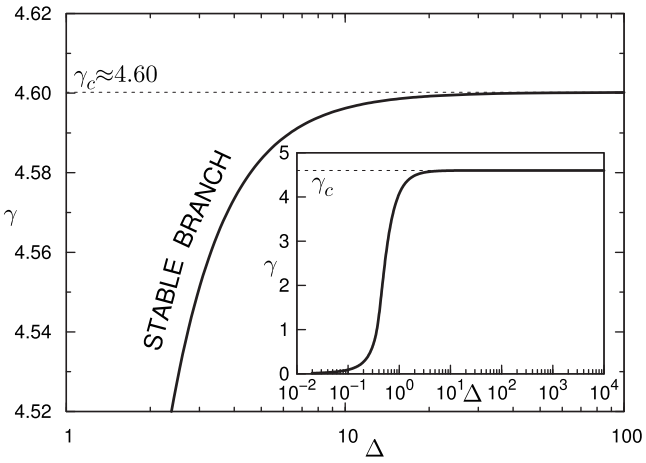


FIG. 14. Connectivity $\gamma$ vs width of the distribution of effective fields $\Delta$ in quantum Model B. The main figure shows $\gamma(\Delta)$ in the region close to critical. Since $\gamma(\Delta)$ is monotonic, there is only a stable branch. The inset shows $\gamma(\Delta)$ in a wider range. As $\gamma$ approaches $\gamma_c$ the value of $\Delta$ increases to infinity continuously.

$$\mathcal{F}^{(B)}[P_+(h)] = \gamma \int \{d\eta_\ell\} \prod_{\ell=1}^{K} R(\eta_\ell)\left(2 \min_{\ell=1,\ldots,K}\{\eta_\ell\}\right) - \int dh_1 dh_2 \mathcal{L}(h_1,h_2) \times \int \frac{d\omega_1 d\omega_2}{2\pi} e^{i\omega_1 h_1 + i\omega_2 h_2} \tilde{\Sigma}(\omega_1,\omega_2), \tag{86}$$

where the expressions for $\mathcal{L}(h_1,h_2)$ and $\tilde{\Sigma}(\omega_1,\omega_2)$ are

$$\mathcal{L}(h_1,h_2) = \max(|h_1-h_2|, \Gamma-\bar{h}), \tag{86a}$$

$$\tilde{\Sigma}(\omega_1,\omega_2) = \tilde{P}_+(\omega_1)\tilde{P}_+(\omega_2)[1-\ln\tilde{P}_+(\omega_1)-\ln\tilde{P}_+(\omega_2)] \tag{86b}$$

[$\tilde{P}(\omega)$, as usual, denotes the Fourier transform of $P(h)$].

The distribution $R(\eta)$ that enters on the right-hand side of Eq. (86) may be related to $P_+(h)$ as follows:

$$R(\eta) = \int dh_1 dh_2 P_+(h_1)P_+(h_2) \times \delta(\eta - (\max(\Gamma/2,h_1)-h_2)_+). \tag{87}$$

The numerical results for quantum Model B are presented in Figs. 14 and 15. In contrast to classical Model B, $\gamma(\Delta)$ is a monotonically increasing function of $\Delta$ (see Fig. 14). Its inverse $\Delta(\gamma)$ is a single-valued function exhibiting no discontinuities. It diverges as $\gamma$ approaches $\gamma_c$. It is fortunate that there is a single branch, as the stability analysis is more complicated in the quantum case.

In Fig. 15, we plot $\|\mathcal{A}\|/N$: the norm of the matrix describing the connectivity of solutions. It is seen that this quantity does not go to zero as $\gamma \to \gamma_c$. This can be explained by the effect of small clusters in a random hypergraph associated with an instance. This hypergraph is a collection of isolated clusters: a giant cluster of size $O(N)$ and a large $[O(N)]$

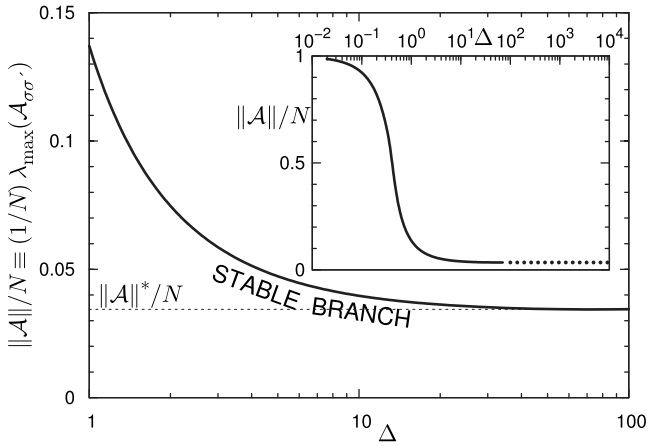


FIG. 15. The norm (largest eigenvalue) of matrix $\mathcal{A}$, defined by Eq. (82), as a function of Δ. The main figure shows the dependence in the critical region, while a wider range of Δ is used for the inset. There is only a stable branch. Values of $\|\mathcal{A}\|$ that could not be computed reliably for very large Δ are estimated using extrapolation, which is indicated by the use of black dotted line.

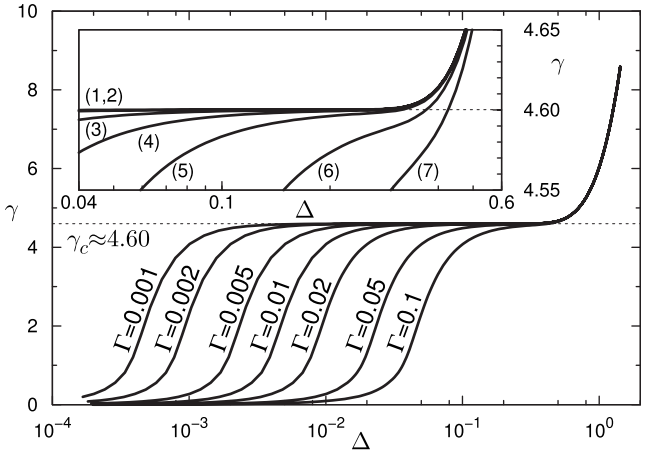


FIG. 16. The dependence $\gamma(\Delta)$ in quantum Model AB for a range of transverse magnetic fields. Curves labeled (1)–(7) in the inset correspond to transverse fields Γ=0.001, 0.002, 0.005, 0.01, 0.02, 0.05, and 0.1, respectively. The curves in the main figure are explicitly labeled with values of Γ. The curves smoothly interpolate between the regime of Model B [$\Delta = O(\Gamma)$] and that of Model A [$\Delta = O(1)$]. In contrast to the classical case, the functions $\gamma(\Delta)$ are monotonic and free of singularities.

number of small clusters. Each cluster may be used to define a subinstance of the problem. The space of solution of the large instance is a Cartesian product of spaces of solutions of subinstances. It can be shown that the norm $\|\mathcal{A}\|$ for the full instance may be written as a sum of norms $\|\mathcal{A}_k\|$ for all the subinstances corresponding to isolated clusters. The large number of small clusters contributes to the finite value of $\|\mathcal{A}\|$ as $\gamma \to \gamma_c$.

We should mention that the computed value of $F^{(B)}$ is not quantitatively correct even in the regime where the replica-symmetric solution is stable. This is due to our making a static approximation. Although quantum Model B describes the limit $\Gamma \to 0$, the static approximation requires a stronger condition $\beta\Gamma \to 0$ in order to be exact. We however work in the opposite limit $\beta\Gamma \to \infty$.

Numerical results for quantum Model AB are presented in Fig. 16. We plot $\gamma(\Delta)$ for a transverse field Γ ranging from Γ=0.001 to Γ=0.1. It can be seen that the functions $\gamma(\Delta)$ are always monotonic. In contrast to classical Model AB, the free energy does not exhibit nonanalytic behavior. The continuous phase transition present for Γ=0 disappears and is instead replaced by a smooth crossover for arbitrarily small Γ>0 as depicted in Fig. 17. The effect of the critical point ($\gamma=\gamma_c, \Gamma=0$) is that the width of the transition $\Delta\gamma$ goes to zero together with Γ.

We conjecture, by analogy with quantum phase transitions in physical systems, that the characteristic width of the transition scales as some power of Γ:

$$\Delta\gamma \propto \Gamma^{1/z}. \tag{88}$$

The width of the transition has been formally defined as follows:

$$\Delta\gamma = \Delta_* \min_{\Delta} \left[ \frac{d\gamma}{d\Delta} \right], \tag{89}$$

where $\Delta_*$ corresponds to the minimum of $d\gamma/d\Delta$. The power law (88) may be verified by plotting points ($\Delta\gamma$ and Γ) on a log-log plot (see Fig. 18). For small Γ, the data seem to converge to power-law scaling with scaling exponent $z=1$ (the slope corresponding to $z=1$ is indicated with the gray solid line). However, we have not studied this scaling dependence analytically and cannot completely rule out the possibility that the dependence of the width of the transition on Γ is more complex and cannot be described by a simple power law.

## VII. CONCLUSION

The main result of this paper is that the thermodynamic phase transition between SAT and UNSAT phases in the classical random *K*-satisfiability problem does not survive when quantum effects are incorporated via coupling to the external transverse magnetic field. We have studied the free energy as a function of connectivity $\gamma$ for different values of the transverse field Γ. The case Γ=0 corresponds to the purely classical limit, and there exists a phase transition when $\gamma$ is

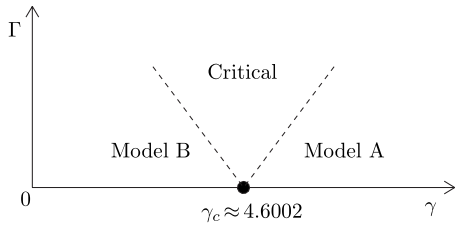


FIG. 17. Illustration of crossover transition for quantum *K*-SAT. The sharp phase transition predicted in classical *K*-SAT is the critical point at Γ=0. For small but nonzero values of Γ it is replaced by a smooth crossover transition of finite width between the underconstrained ($\gamma < \gamma_c$) regime described by Model B and the overconstrained ($\gamma > \gamma_c$) regime described by Model A. The width of the critical region decreases as $\Gamma \to 0$.

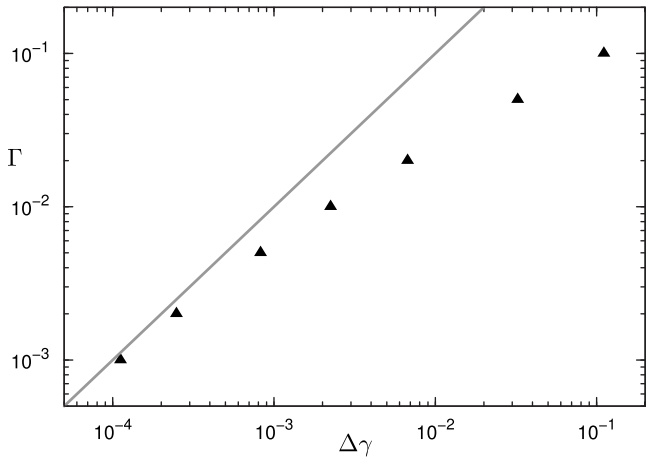


FIG. 18. Transverse field $\Gamma$ vs the width of the transition $\Delta\gamma$. A log-log scale is used to obtain a power-law fit between the width of the transition and the transverse field $\Gamma=(\Delta\gamma)^z$. Solid triangles correspond to numerical estimates of $\Delta\gamma$ for the following values of $\Gamma$: 0.001, 0.002, 0.005, 0.01, 0.02, 0.05, and 0.1. The slope of the gray solid line corresponds to $z=1$.

crossing its critical value. We have demonstrated that for any small value of $\Gamma$ the free energy becomes analytic and the sharp phase transition at $\Gamma=0$ is replaced by a smooth crossover transition. This stands in contrast to the classical *K*-satisfiability model at finite temperatures, where we have found a first-order phase transition line on the temperature-connectivity plane approaching continuously a zero-temperature limit. However, it is not inconceivable that the seeming difference between the classical and quantum cases is an artifact of the replica-symmetric approximation. The RSB analysis of dilute antiferromagnetic Potts glass at finite temperature indicates that the analogous zero-temperature static transition becomes a smooth crossover at finite temperature [57]. Whether the inclusion of RSB in $T>0$ classical *K*-SAT will similarly lead to the smoothing of the static transition is open to investigation.

We believe the above-mentioned phenomenon is not universal among dilute long-range spin glasses. We expect that in models with Ising or *p*-spin interactions the phase transition at $\gamma=\gamma_c$ is not affected by transverse fields below a certain threshold ($\Gamma<\Gamma_c$) and that the phase boundary has the form of the line labeled (1) in Fig. 1. We attribute the difference to the fact that constraints involved in Viana-Bray and dilute *p*-spin models are "stronger" (i.e., a greater number of spin combinations are penalized) than those in *K*-satisfiability.

The limitations of our approach are the assumptions of the replica symmetry and the failure to include the time dependence of correlation functions. The latter approximation has been justified on the ground that we work in the limit of small transverse fields, as we establish the absence of a phase transition line on the $(\gamma,\Gamma)$ plane. It is known that the replica-symmetric approximation can capture the existence of the thermodynamic transition in the classical *K*-satisfiability model while providing an overestimated value for the transition point (critical connectivity).

Previously, we attempted to analyze the $O(\Gamma)$ corrections to the free energy of the $\Gamma=0$ (classical) *K*-SAT problem along similar lines [58]. In contrast to the present analysis, we computed corrections to the integer-$\delta$-peak solution (12) of zero-temperature classical *K*-SAT developed in Ref. [23]. Although the assumption of integer values of the effective fields is more natural for $T=0$, $\Gamma=0$ and has been used to construct an RSB theory of $T=0$ *K*-SAT [25], at the replica-symmetric level it does not give a truly stable solution for either $T>0$ or $\Gamma>0$. At the same time, the solution derived in the present paper is globally stable in the RS sector at finite temperatures and transverse fields.

To obtain a correct location of the phase transition one needs to take into account the spontaneous breaking of the replica symmetry [25]. However, we hope that our main result—the smoothing of the phase transition at finite values of the transverse field—will be immune to the effects of the replica symmetry breaking. On the other hand, it is well known that the replica-symmetric approximation fails to account for the dynamic transition and the complex structure of local minima existing in the classical *K*-satisfiability model at connectivity that is smaller than that of the static transition. From the perspective of the quantum adiabatic algorithm, the likely conclusion is that the bottleneck of the QAA may be in this dynamic transition rather than the static transition. Recent results on *K*-SAT show the presence of another transition: the so-called condensation transition (which coincides with the dynamic transition for $K=3$) [27,28]. It is believed that the crossover to the exponential complexity of the classical algorithm happens at the condensation transition. It may also be relevant for the performance of quantum adiabatic family of algorithms.

Since the nonanalytic behavior of the free energy associated with the static transition is the isolated singularity, it should be irrelevant to the complexity of the QAA except when $\gamma=\gamma_c$ precisely. It is conceivable that the complexity of the QAA will be subexponential for $\gamma\neq\gamma_c$ if singularities of the free energy associated with, e.g., the condensation transition are weaker than that of static (satisfiability) transition.

The analysis of a quantum version of the *K*-satisfiability problem led us to a reexamination of the static phase transition in the zero-temperature classical limit. In Ref. [23] it has been predicted, using a replica-symmetric analysis, that this phase transition is of a random first order (discontinuous) type. We have found that the transition is, in fact, of second order (continuous). In the vicinity of the phase transition, the functional order parameter is given by the new scale-free solution that we described in Sec. V. This second-order transition is of a peculiar nature, as it possesses critical exponents typically associated with first-order phase transitions. Consequently, numerical studies must be performed with care as finite-size effects can make this phase transition indistinguishable from a first-order transition.

We have found that in the vicinity of the transition the singular component of the free energy is $F_{\text{sing}}\sim\frac{t}{\ln t}$ where $t=\gamma-\gamma_c$. The logarithmic correction is sufficient to make the first derivative $dF/d\gamma$ continuous; therefore, there is no associated "latent heat." Ordinarily, finite "latent heat" must be a continuous function of thermodynamic variables, which ensures that the phase transition persists for finite $\Gamma$, at least up to the critical point. Conversely, when it is zero, it is plausible that the phase transition might disappear for arbitrarily small $\Gamma$ as we claim.

Throughout the paper we have attempted to keep the discussion as general as possible. All formulas derived using the replica method can be applied to a host of spin-glass models defined on random hypergraphs. In the analysis presented in the paper it will usually involve the replacement of the cost function $E_J(s_1,\ldots,s_K)$ by a suitable expression and performing disorder averages $\langle\cdots\rangle_J$ appropriately. Quantum analogs of dilute $p$-spin [55], $K$-NAE-SAT [59], the exact cover [30,60,61], and the vertex cover [62] problems can be studied using this method.

We have also devised a new method, of quasi–Monte Carlo variety, for the numerical determination of the functional order parameter. Since it significantly outperforms standard the Monte Carlo method, it can be used to improve the accuracy in the numerical studies of one-step replica symmetry breaking, which so far required significant numerical effort [63].

For future work it is of interest to investigate the stability region of the replica-symmetric solution on the plane $(\gamma,\Gamma)$ in a quantum regime corresponding to finite values of $\Gamma$. In the classical case $\Gamma=0$, the replica-symmetric solution loses the stability at the point of the dynamic (replica symmetry breaking) transition $\gamma=\gamma_d$. Beyond this point the energy landscape is characterized by a proliferation of an exponentially large (in $N$) number of deep local minima in the energy landscape, which traps classical annealing algorithms. It is of interest to explore how this picture is modified for finite values of $\Gamma$. The structure of the free-energy landscape will have implications for the scaling of the minimum gap in the QAA.

The effective classical Hamiltonian (44) may be used as a starting point for performing RSB analysis. Although it reflects the static approximation, the disorder dependence is explicit. The replica-symmetric ansatz that we made corresponds to the assumption that the distributions of magnetizations on different sites are not correlated. In the limit of small $\Gamma$ relevant local minima correspond to integer values of magnetizations: $m\approx\pm 1$ and $m\approx 0$. Although local minima with intermediate values of $m$ exist, our analysis indicates that corresponding free energies correspond to excitations with energies much larger than the typical $O(\Gamma)$. In this limit, continuous magnetizations may be replaced by discrete variables taking three possible values. The third possibility ($m=0$) makes the problem distinctly different from the classical $K$-SAT.

## ACKNOWLEDGMENTS

We acknowledge the financial support of the U.S. National Security Agency's Laboratory for Physical Sciences. We would also like to thank Lenka Zdeborová from the Laboratoire de Physique Théorique et Modeles Statistiques, Universite Paris-Sud for interesting and useful comments.

## APPENDIX: QUASI–MONTE CARLO IMPLEMENTATION

The quasi–Monte Carlo (QMC) method of evaluating integrals replaces the random sequences of standard MC algorithms with deterministic minimum discrepancy sequences [64]. For example, a two-dimensional integral of a function $f(x,y)$ on $[0;1]^2$ is approximated by

$$\int_{[0;1]^2} dx\,dy f(x,y) \approx \frac{1}{N-1}\sum_{k=1}^{N-1} f\left(\frac{i_k}{N},\frac{j_k}{N}\right), \tag{A1}$$

where $\{i_k,j_k\}_{k=1}^{N-1}$ is the minimum discrepancy sequence (since it is a finite, we will call it a minimum discrepancy set). We use Sobol sequences [65] and choose $N$ to be an integer power of 2 for best results. The error estimate for the two-dimensional integral (A1) is $O(\log N/N)$ for continuous functions $f(x,y)$ and $O(1/N^{2/3})$ for discontinuous functions $f(x,y)$. This compares favorably to the expected error of $O(1/N^{1/2})$ in the standard Monte Carlo method.

We adapt the QMC method to integrals involving univariate probability distributions. The probability distributions will be represented internally as a finite-size sample. In contrast to the standard MC method, we will ensure that these samples are as uniform as possible. With each univariate distribution $p(x)$ we associate a function $X(p)$ defined on the interval $[0;1]$ and satisfying the condition

$$X\left(\int_{-\infty}^{x} dx' p(x')\right) = x. \tag{A2}$$

Internally, it will be represented by a set of $\{X_k\}_{k=1}^{N-1}$, where $X_k=X(k/N)$.

For an arbitrary function $\lambda(x)$, its expectation value may be approximated by

$$\int dx\, p(x)\lambda(x) = \frac{1}{N-1}\sum \lambda(X_i). \tag{A3}$$

The flow of the computation shall consist of a sequence of transformations of probability distributions. The elementary operation is finding the distribution of a variable $z=f(x,y)$, given distributions of variables $x$ and $y$:

$$p(z) = \int dx\,dy p(x)p(y)\delta(z-f(x,y)). \tag{A4}$$

That is, we need to find a uniform sample $\{Z_k\}$ of a distribution $p(z)$ from uniform samples $\{X_k\}$ and $\{Y_k\}$ of distributions $p(x)$ and $p(y)$. What the appropriate sample should be can be assessed indirectly by considering the expectation value of an arbitrary function $\lambda(z)$:

$$\frac{1}{N-1}\sum_{k=1}^{N-1}\lambda(Z_k) = \int dz\, p(z)\lambda(z) = \int dx\,dy\, p(x)p(y)\lambda(f(x,y))$$

$$= \int_{[0;1]^2} dp_1 dp_2 \lambda(f(X(p_1),Y(p_2))). \tag{A5}$$

Using (A1) to estimate the integral over $[0;1]^2$ in (A5), we may write

$$\frac{1}{N-1}\sum_k \lambda(Z_k) = \frac{1}{N-1}\sum_k \lambda(f(X_{i_k},Y_{j_k})), \tag{A6}$$

where $\{i_k,j_k\}_{k=1}^{N-1}$ is the Sobol set. The choice of the sample $\{Z_k\}$ satisfying (A6) for any $\lambda(z)$ is unique. Algorithmically, it is computed as follows:

(i) For $k=1,\ldots,N-1$, evaluate $Z_k=f(X_{i_k},Y_{j_k})$, where $\{i_k,j_k\}_{k=1}^{N-1}$ is the Sobol set.

(ii) Sort the resulting vector $\{Z_k\}_{k=1}^{N-1}$ in increasing order.

The last step is to ensure that $Z_k<Z_{k+1}$, which is required by definition (A2).

### 1. Application to $T=0$ classical 3-SAT

Let us briefly describe how this idea can be applied to solving self-consistency equations. For $K=3$, the equation for $Q(u)$ already has the form of (A4),

$$Q(u)=\int dh_2 dh_3 P(h_2)P(h_3) \times \delta(u+J_1\min(1,(J_2h_2)_+,(J_3h_3)_+)), \tag{A7}$$

enabling one to compute $\{u_k\}$ from $\{h_k\}$. The equation for $P(h)$ may be written as follows:

$$P(h)=\sum_{d=0}^{\infty} f_d(3\gamma)P_d(h), \tag{A8a}$$

$$P_d(h)=\int \{du_k\}\prod_{k=1}^{d} Q(u_k)\,\delta\left(h-\sum_k u_k\right). \tag{A8b}$$

A set of $\{P_d(h)\}$ is computed using the following recursive definition having the desired form of (A4):

$$P_d(h)=\int dh'du P_{d-1}(h')Q(u)\,\delta(h-h'-u), \tag{A9}$$

together with the condition $P_0(h)=\delta(h)$. The distribution $P_0(h)$ is represented by a vector of $N-1$ zeros. Computing a sample of $P(h)$ from a set of samples of $P_d(h)$ via (A8a) means that we have to select $N-1$ values from the larger set of $(d_{\max}+1)\times(N-1)$ values that represent distributions $P_0(h)$ through $P_{d_{\max}}(h)$.

The elegant way to accomplish it is the following. We formally introduce the function $H(t,p)$ defined on $[0;1]^2$. For any fixed value of $t$, viewed as a function of one argument $p$, $H(t,p)$ represents the distribution $P_{d(t)}(h)$:

$$H\left(\int_{-\infty}^{h} dh' P_{d(t)}(h')\right)=p \tag{A10}$$

and $d(t)$ is a stepwise function of $t$ such that

$$\sum_{k=0}^{d(t)} f_k(3\gamma)\leqslant t<\sum_{k=0}^{d(t)+1} f_k(3\gamma). \tag{A11}$$

The expectation value of an arbitrary function $\lambda(h)$ can be written as

$$\int dh\, P(h)\lambda(h)=\int_{[0;1]^2} dt\, dp\, \lambda(H(t,p)). \tag{A12}$$

Applying (A1) to the integral, we construct the sample for $P(h)$ from $\{h_{j_k}^{(d(i_k))}\}$, where $\{h_k^{(d)}\}$ represents the sample for $P_d(h)$.

Memory requirements for each iteration step can be kept at $O(N)$, whereas the time complexity is $O(N\log^2 N)$, which is the product of $d_{\max}=O(\log N)$ and the $O(N\log N)$ complexity of sorting.

The procedure described above is trivially extended to $K\geqslant 4$ and to finite temperatures $T>0$. The extension to finite temperatures merely changes the form of $u_J(h_2,\ldots,h_K)$. The distribution $Q(u)$ may be computed using either a single $(K-1)$-dimensional integral or as a sequence of $K-2$ two-dimensional integrals. The latter approach is possible because for any $K\geqslant 4$, the function $u_J(h_2,\ldots,h_K)$ may be written in terms of compositions of functions of two variables.

Instead of iterating the self-consistency equations for a fixed value of $\gamma$, we achieve accelerated convergence by specifying the desired width $\Delta$ of the distribution $P(h)$ and adjusting the value of $\gamma$ at each iteration step to satisfy this constraint. As a result, we observe exponentially fast convergence and avoid the effects of the critical slowing down in the vicinity of the phase transition.

### 2. Application to quantum $K$-SAT

The case of quantum $K$-SAT in the limit $\Gamma\ll 1$ is slightly more involved. The order parameter is the joint probability distribution (JPD) $P(h,\bar{h})$. For quantum Model B, it is possible to parameterize this JPD by a univariate distribution $P_+(h)$ and apply the method described previously. For quantum Model AB, however, no such parametrization is possible.

One possible solution is to work with univariate distributions $Q(u)$ and $R(\eta)$ exclusively. It is straightforward to compute $Q(u)$ from $R(\eta)$ by evaluating the $(K-1)$-dimensional integral (61a)–(61c), which can be further reduced to the sequence of two-dimensional integrals for $K\geqslant 4$. The nontrivial part is the computation $R(\eta)$ from $Q(u)$, which we describe below.

It is easy to see that $Q(u)$ is symmetric [i.e., $Q(u)=Q(-u)$] and that $|u|\leqslant 1$. Let $\xi_{1/2}$ denote the probability that $|u|>1/2$:

$$\xi_{1/2}=\int_{|u|>1/2} du\, Q(u). \tag{A13}$$

We introduce the reduced distributions $\hat{Q}_<(u)$ and $\hat{Q}_>(u)$ defined on intervals $[0;1/2]$ and $[-1;-1/2]$, respectively:

$$\hat{Q}_<(u)=\frac{2}{1-\xi_{1/2}}Q(u)\,\theta(u)\,\theta\left(\frac{1}{2}-u\right), \tag{A14a}$$

$$\hat{Q}_>(u)=\frac{2}{\xi_{1/2}}Q(u)\,\theta(-u)\,\theta\left(-\frac{1}{2}-u\right), \tag{A14b}$$

Where

$$\theta(x)=\begin{cases}1 & \text{for } x>0,\\ 0 & \text{for } x\leqslant 0\end{cases}$$

is the Heaviside function. The factors $2/(1-\xi_{1/2})$ and $2/\xi_{1/2}$ ensure that $\hat{Q}_<(u)$ and $\hat{Q}_>(u)$ are normalized to unity.

We also define

$$\hat{P}_0(h) = \sum_{d=0}^{\infty} f_d\left(\frac{K\gamma}{2}(1-\xi_{1/2})\right) \times \int \{du_k\} \prod_{k=1}^{d} \hat{Q}_<(u_k)\,\delta\left(h - \sum_k u_k\right), \quad \text{(A15)}$$

as well as the sequence $\{\hat{P}_k(h)\}$: the sequence of successive convolutions of $\hat{P}_0(h)$ with $\hat{Q}_>(u)$. It is computed via the recurrence relation

$$\hat{P}_k(h) = \int du\, \hat{Q}_>(u)\hat{P}_{k-1}(h-u). \quad \text{(A16)}$$

The distribution $\hat{P}_k(h)$ gives the contribution from vertices that have an arbitrary number of incident hyperedges with $u \in [0;1/2]$ and precisely $k$ hyperedges with $u \in [-1;-1/2]$. In view of a relation (55) between $\bar{u}$ and $u$, to each $h$ in the distribution $\hat{P}_k(h)$ there corresponds $\bar{h}=k+h$.

Including contributions from mirror image regions $u \in [-1/2;0]$ and $u \in [1/2;1]$, the distribution $P(h,\bar{h})$ may be written in terms of $\{\hat{P}_k(h)\}$:

$$P(h,\bar{h}) = \sum_{k_+,k_- \geqslant 0} f_{k_+}\left(\frac{K\gamma}{2}\xi_{1/2}\right) f_{k_-}\left(\frac{K\gamma}{2}\xi_{1/2}\right) \times \int dh_+ dh_- \hat{P}_{k_+}(h_+)\hat{P}_{k_-}(h_-) \times \delta(h - h_+ + h_-)\,\delta(\bar{h} - k_+ - k_- - h_+ - h_-), \quad \text{(A17)}$$

where $f_k(\alpha)$ denotes the Poisson distribution with mean $\alpha$ as usual. It follows that the distribution $R(\eta)$ given by Eq. (87) may be written in the following general form:

$$R(\eta) = \int dt_+ dt_- dh_+ dh_- \hat{P}_{k(t_+)}(h_+)\hat{P}_{k(t_-)}(h_-) \times \delta(\eta - f_{k(t_+),k(t_-)}(h_+,h_-)), \quad \text{(A18)}$$

where $f_{k_+,k_-}(h_+,h_-) = \eta(h_+ - h_-, \Gamma - k_+ - k_- - h_+ - h_-)$ and we have defined a stepwise function $k(t)$ chosen to satisfy

$$\sum_{r=0}^{k(t)} f_\ell\left(\frac{K\gamma}{2}\xi_{1/2}\right) \leqslant t < \sum_{r=0}^{k(t)+1} f_\ell\left(\frac{K\gamma}{2}\xi_{1/2}\right). \quad \text{(A19)}$$

Once $R(\eta)$ has been expressed as a four-dimensional integral, the values $\{\eta_k\}_{k=1}^{N-1}$ may be sampled using Sobol sets. Memory and time requirements of this procedure remain $O(N)$ and $O(N \log^2 N)$, respectively.


[1] A. Osterloh, L. Amico, G. Falci, and R. Fazio, Nature (London) **416**, 608 (2002).
[2] J. Brooke, T. F. Rosenbaum, and G. Aeppli, Science **284**, 779 (1999).
[3] G. Santoro, R. Martonak, E. Tosatti, and R. Car, Science **295**, 2427 (2002).
[4] R. Schützhold and G. Schaller, Phys. Rev. A **74**, 060304(R) (2006).
[5] M. C. Bañuls, R. Orús, J. I. Latorre, A. Pérez, and P. Ruiz-Femenía, Phys. Rev. A **73**, 022344 (2006).
[6] T. Caneva, R. Fazio, and G. E. Santoro, Phys. Rev. B **76**, 144427 (2007).
[7] T. Kadowaki and H. Nishimori, Phys. Rev. E **58**, 5355 (1998).
[8] E. Farhi, J. Goldstone, S. Gutmann, J. Lapan, A. Lundgren, and D. Preda, Science **292**, 472 (2001).
[9] A. Messiah, *Quantum Mechanics* (North-Holland, Amsterdam, 1966), Vol. 1.
[10] M. Mézard and G. Parisi, J. Phys. (France) Lett. **46**, L771 (1985).
[11] Y. Fu and P. W. Anderson, J. Phys. A **19**, 1605 (1986).
[12] M. Mézard, G. Parisi, and M. Virasoro, *Spin Glass Theory and Beyond* (World Scientific, Singapore, 1987).
[13] M. R. Garey and D. S. Johnson, *Computers and Intractability: A Guide to the Theory of NP-Completeness* (Freeman, New York, 1997).
[14] *Lectures in the Sciences of Complexity*, edited by D. L. Stein (Addison-Wesley, New York, 1989).
[15] S. Kirkpatrick and B. Selman, Science **264**, 1297 (1994).
[16] Special issue on *Phase Transitions and The Search Problem*, edited by T. Hogg, B. A. Huberman, and C. Williams, Artif. Intell. 81(1–2) (1996).
[17] Special issue on *NP-hardness and Phase Transitions*, edited by O. Dubois, R. Monasson, B. Selman, and R. Zecchina, Theor. Comput. Sci. 265(1–2) (2001).
[18] A. Percus, G. Istrate, and C. Moore, *Computational Complexity and Statistical Physics* (Oxford University Press, New York, 2006).
[19] R. Monasson, R. Zecchina, S. Kirkpatrick, B. Selman, and L. Troyansky, Nature (London) **400**, 133 (1999).
[20] S. Bravyi, e-print arXiv:quant-ph/0602108.
[21] D. Sherrington and S. Kirkpartick, Phys. Rev. Lett. **35**, 1792 (1975).
[22] R. Monasson and R. Zecchina, Phys. Rev. Lett. **76**, 3881 (1996).
[23] R. Monasson and R. Zecchina, Phys. Rev. E **56**, 1357 (1997).
[24] M. Mézard, G. Parisi, and R. Zecchina, Science **297**, 812 (2002).
[25] M. Mézard and R. Zecchina, Phys. Rev. E **66**, 056126 (2002).
[26] M. Mézard and G. Parisi, J. Stat. Phys. **111**, 1 (2003).
[27] F. Krzakała, A. Montanari, F. Ricci-Tersenghi, G. Semerjian, and L. Zdeborová, Proc. Natl. Acad. Sci. U.S.A. **104**, 10318 (2007).
[28] A. Montanari, F. Ricci-Tersenghi, and G. Semerjian, J. Stat. Mech.: Theory Exp. p04004 (2008).
[29] V. N. Smelyanskiy, S. Knysh, and R. D. Morris, Phys. Rev. E **70**, 036702 (2004).

[30] S. Knysh, V. N. Smelyanskiy, and R. D. Morris, e-print arXiv:quant-ph/0403416.
[31] T. Yamamoto and H. Ishii, J. Phys. C **20**, 6053 (1987).
[32] D. Thirumalai, Q. Li, and T. R. Kirkpatrick, J. Phys. A **22**, 3339 (1989).
[33] Y. Y. Goldschmidt and P.-Y. Lai, Phys. Rev. Lett. **64**, 2467 (1990).
[34] J. Miller and D. A. Huse, Phys. Rev. Lett. **70**, 3147 (1993).
[35] J. Ye, S. Sachdev, and N. Read, Phys. Rev. Lett. **70**, 4011 (1993).
[36] A. J. Bray and M. A. Moore, J. Phys. C **13**, L655 (1980).
[37] Y. Y. Goldschmidt, Phys. Rev. B **41**, 4858 (1990).
[38] B. M. McCoy and T. T. Wu, Phys. Rev. **176**, 631 (1968); **188**, 1014 (1969).
[39] D. S. Fisher, Phys. Rev. B **50**, 3799 (1994); **51**, 6411 (1995).
[40] A. Montanari and G. Semerjian, J. Stat. Phys. **124**, 103 (2006).
[41] A. B. Harris, J. Phys. C **7**, 3082 (1974).
[42] S. Sachdev, *Quantum Phase Transitions* (Cambridge University Press, Cambridge, England, 1999).
[43] W. Van Dam, M. Mosca, and U. Vazirani, *Proceedings of the 42nd Annual Symposium on Foundations of Computer Science*, (IEEE Computer Society, Washington, DC. USA, 2001), p. 279.
[44] E. Farhi, J. Goldstone, and S. Gutmann, e-print arXiv:quant-ph/0201031.
[45] A. Boulatov and V. N. Smelyanskiy, Phys. Rev. A **68**, 062321 (2003).
[46] I. Kanter and H. Sompolinsky, Phys. Rev. Lett. **58**, 164 (1987).
[47] L. Viana and A. J. Bray, J. Phys. C **18**, 3037 (1985).
[48] J. R. L. de Almeida, C. De Dominicis, and P. Mottishaw, J. Phys. A **21**, L693 (1988).
[49] B. K. Chakrabarti, A. Dutta, and P. Sen, *Quantum Ising Phases and Transitions in Transverse Ising Models* (Springer-Verlag, Heidelberg, 1996).
[50] P. Ray, B. K. Chakrabarti, and A. Chakrabarti, Phys. Rev. B **39**, 11828 (1989).
[51] J. Zinn-Justin, *Quantum Field Theory and Critical Phenomena* (Clarendon Press, Oxford, 1989).
[52] See EPAPS Document No. E-PLEEE8-78-002811 for the mathematical details of replica calculations and the description of Bethe-Peierls approximation and quantum belief propagation equations. For more information on EPAPS, see http://www.aip.org/pubservs/epaps.html.
[53] H. Bethe, Proc. R. Soc. London, Ser. A, **150**, 552 (1935); R. Peierls, *ibid.* **154**, 207 (1936).
[54] W. T. Eadie *et al.*, *Statistical Methods in Experimental Physics* (North-Holland, Amsterdam, 1971).
[55] M. Mézard, F. Ricci-Tersenghi, and R. Zecchina, J. Stat. Phys. **111**, 505 (2003).
[56] B. Bollobás, *Random Graphs* (Academic Press, London, 1985).
[57] F. Krzakała and L. Zdeborová, Europhys. Lett. **81**, 57005 (2008).
[58] S. Knysh and V. N. Smelyanskiy, e-print arXiv:cond-mat/0602257.
[59] D. Achlioptas, A. Chtcherba, G. Istrate, and C. Moore, in *Proceedings of 12th Annual Symposium on Discrete Algorithms* (SIAM, Philadelphia, 2001), p. 279.
[60] V. Kalapala and C. Moore, e-print arXiv:cs.CC/0508037.
[61] J. Raymond, A. Sportiello, and L. Zdeborová, Phys. Rev. E **76**, 011101 (2007).
[62] M. Weigt and A. K. Hartmann, Phys. Rev. Lett. **84**, 6118 (2000).
[63] S. Mertens, M. Mézard, and R. Zecchina, Random Struct. Algorithms **28**, 340 (2006).
[64] H. Niederreiter, *Random Number Generation and Quasi-Monte Carlo Methods* (SIAM, Philadelphia, 1992).
[65] W. H. Press *et al.*, *Numerical Recipes: the Art of Scientific Computing* (Cambrige University Press, Cambridge, England, 1986).